




# Elucidating the antiviral effects of a novel compound throat anti-viral through metabolomics and network pharmacology: A study on infectious bronchitis virus in poultry

Huixin Liu<sup>a</sup>, Xiaofang Wei<sup>a</sup>, Yang He<sup>a</sup>, Sijia Pan<sup>a</sup>, Chenchen Wang<sup>a</sup>, Junze Cheng<sup>a</sup>, Qiyuan Zhao<sup>a</sup>, Kaichuang Shi<sup>a,b</sup>, Hongbin Si<sup>a,\*</sup> 

<sup>a</sup> College of Animal Science and Technology, Guangxi Key Laboratory of Animal Breeding, Disease Control and Prevention, Guangxi grass station, Guangxi University, Nanning, 530004, Guangxi, China

<sup>b</sup> Guangxi Center for Animal Disease Control and Prevention, Nanning 530001, China

## ARTICLE INFO

### Keywords:

Infectious bronchitis virus  
Compound throat anti-viral  
*In vitro* and *in vivo* studies  
FoxO signaling pathway  
Antiviral efficacy

## ABSTRACT

Infectious bronchitis virus (IBV) is a major pathogen that causes significant economic losses in the global poultry industry. Current vaccination strategies provide only partial protection, highlighting the need for more effective prevention and treatment methods. This study aimed to develop a novel compound throat anti-viral (CTA) from natural plants using data from the Traditional Chinese Medicine Inheritance System and identification through liquid chromatography-mass spectrometry. CTA demonstrated substantial anti-IBV effects both *in vitro* and *in vivo* studies. *In vitro*, CTA significantly inhibited IBV multiplication and alleviated the pathological lesions in chicken embryonic kidney cells, tracheal rings, and chicken embryos. *In vivo*, a seven-day treatment with CTA obtained much milder clinical signs, enhanced growth performance, and better immune organ indices in infected chickens. Additionally, CTA treatment reduced IBV levels in the trachea and lungs and increased specific antibody titers. CTA also maintained body homeostasis, exhibiting strong antioxidant and anti-inflammatory properties that mitigated respiratory tract damage. Metabolomics and network pharmacology analyses, revealed that CTA's antiviral effects are mediated through the FoxO signaling pathway. This study successfully developed an effective prescription database based on the Traditional Chinese Medicine Inheritance System and validated the antiviral efficacy of CTA through comprehensive *in vitro* and *in vivo* experiments. The findings elucidated the mechanisms of CTA's action, particularly through the FoxO signaling pathway, and highlighted its potential for clinical application as a novel antiviral treatment for IBV in the poultry industry.

## Introduction

Infectious bronchitis virus (IBV) is a highly contagious pathogen, and belongs to the order *Nidovirales*, the family *Coronaviridae*, and the genus *Gammacoronavirus* (Bande et al., 2017). The disease caused by IBV, known as chicken infectious bronchitis, is classified as a Class II infectious disease and has resulted in significant economic losses in the poultry industry (Jackwood, 2012). While chickens are the natural hosts of IBV, it has also been found in pheasants and peacocks (Bande et al., 2005). Chickens of all ages can be affected by IBV, but chicks and laying hens are particularly susceptible (de Wit et al., 2011). Currently, the primary methods used to combat IBV are vaccines, antiviral drugs, and natural plants (Jordan, 2017). Vaccination is an effective means of

preventing IBV (Bijlenga et al., 2004; Valastro et al., 2016). However, due to the presence of numerous IBV serotypes and varying levels of cross-protection between serotypes, current vaccines are not fully effective in IBV prevention and control requirements (Fan et al., 2018; Jordan, 2017). There have also been reports of disease outbreaks in vaccinated chickens (Lin et al., 2016; Lv et al., 2021). Due to the misuse of certain antiviral drugs, there have been instances of viral mutations and concerns regarding veterinary drug residues (Cheung et al., 2006; Pratiwi et al., 2023). As a result, several countries have enforced more stringent regulations on antiviral veterinary medications, adding complexity to the prevention and treatment of IBV (Yuan et al., 2022). In recent years, the use of natural plant compounds in China to prevent and treat IBV has shown promising results. Some examples include Maxing

\* Corresponding author.

E-mail address: [shb2009@gxu.edu.cn](mailto:shb2009@gxu.edu.cn) (H. Si).

<https://doi.org/10.1016/j.psj.2025.104956>

Received 4 January 2025; Accepted 26 February 2025

Available online 1 March 2025

0032-5791/© 2025 The Authors. Published by Elsevier Inc. on behalf of Poultry Science Association Inc. This is an open access article under the CC BY-NC-ND license (<http://creativecommons.org/licenses/by-nc-nd/4.0/>).

Shigan Decoction, Shuanghuanglian Oral Liquid, Shigan Dilong Granules, and Cangpu Oral Liquid (Chen et al., 2019a; Chen et al., 2022; Feng et al., 2021; Peng et al., 2022a; Wang and Liu, 2014; Wiseman, 2002; Xiang et al., 2023; Yin et al., 2011). However, despite these advancements, there are still challenges in preventing and controlling IBV on a larger scale, especially in the context of intensive breeding (Dhama et al., 2014). Additionally, further research is needed to fully understand the drug action mechanism of these natural plant compounds.

The Traditional Chinese Medicine Inheritance Computing System V3.0 (TCMICS V3.0) is an information system that integrates traditional Chinese medicine knowledge and data (Ren et al., 2023). Its objective is to utilize modern technology to preserve, analyze, and apply classical Chinese medicine theory and clinical practice knowledge, thus supporting the teaching, research, and international exchange of Chinese medicine (Liu et al., 2022). Additionally, the platform aims to promote the integration and development of traditional medicine and modern technology. To identify a natural plant compound composition for the rapid treatment of chicken infectious bronchitis, this study utilized the TCMICS V3.0 to construct a database of prescriptions for IBV respiratory diseases. Through in-depth data mining, a new prescription called compound CTA was derived. CTA is a synergistic mixture composed of 18% *Rehmannia glutinosa*, 18% *Fritillaria fritillaria*, 18% *Ophiopogon japonicus*, 14% *licorice*, 14% *borneol*, and 18% *bitter almond*.

This study aimed to evaluate the antiviral activity of CTA against IBV both *in vitro* and *in vivo*. *In vitro* experiments were conducted to determine the safe concentration and effectiveness on CEK cell, as well as the tracheal rings and chicken embryo. The *in vivo* evaluation utilized various indicators, including clinical efficacy, immune organ index, humoral immunity, cellular immunity, and viral RNA amount, to assess the efficacy of CTA. To explore the *in vivo* antiviral mechanism of CTA, non-targeted metabolomic analysis was performed using gas chromatography-mass spectrometry to identify potential biomarkers. Additionally, network pharmacology combined with non-targeted metabolomics was employed to analyze the components of traditional Chinese medicine, effective blood components, and possible signaling pathways to determine the anti-IBV mechanism of CTA *in vivo*. The study results confirmed the significant potential of CTA as a new anti-IBV drug.

## Materials and methods

### Viral strains, embryonated chicken and cell lines

The pathogenic IBV strain M41 (batch number AV1511) was obtained from Professor Mo Meilan of Guangxi University. The strain was propagated three times in specific pathogen-free (SPF) 10-day-old chicken embryos at the Guangxi Veterinary Research Institute in China. The EID<sub>50</sub> of the IBV M41 strain was determined using the Reed-Muench method. The CEK immortalized cell line (Guangzhou Genio Company, Cat No: JNO-Q0017) was used for adaptation of the IBV M41 strain (Liu et al., 2024). The cells were cultured in DMEM (H) medium (Soleba, Cat No: P12100) supplemented with 10% fetal calf serum (HyClone, Cat No: SH30070.03) at a concentration of  $5 \times 10^6$  cells/mL. Subsequently, 0.1 mL of cells was added to each well of a 96-well plate. The culture conditions were maintained at 37°C and 5% CO<sub>2</sub>, and the experiment was initiated once the cell density reached 60%. Based on previous studies, the adaptation and replication time of IBV in chicken embryonic kidney cells were observed for 25-50 hours (Chen et al., 2019b). Afterward, the half-cell culture infectious dose (TCID<sub>50</sub>) of the IBV M41 strain was determined using the Reed-Muench method.

### Generation, preparation and ingredient identification of CTA

Prescriptions for clinical symptoms of IBV were collected from 34,324 Chinese medicine prescription data sets in the Chinese medicine prescription database, and 7,505 traditional Chinese medicine

prescriptions in the cross-retrieval database of traditional Chinese medicine prescriptions. The preparation data set and 33,837 traditional prescriptions, and 4,207 traditional Chinese medicine prescription preparation data sets (from TCMICS V3.0) were used. Prescriptions with similar occurrences to IBV were included in the statistical analysis database. Duplicate data sets were eliminated and the naming of traditional Chinese medicines was standardized. The data from TCMICS V3.0 extracted the prescriptions for cluster analysis (Zhang et al., 2022), generating a combination of core drugs and related ingredients named compound throat anti-viral (CTA). A synergistic mixture of CTA, consisting of 90 g of *Rehmannia glutinosa*, 90 g of *Fritillaria fritillaria*, 90 g of *Ophiopogon japonicus*, 70 g of *licorice*, 70 g of *borneol*, and 90 g of *bitter almond*, was mixed into 500 g and decocted. All purchased medicinal materials were sourced from a reputable traditional Chinese medicine store. For materials that required cutting, an automatic slicer was used to shred them into pieces of approximately 3-5 mm in size. For granular materials, the raw material was used directly. After mixing the medicinal materials according to the prescribed ratio, they were first soaked at room temperature for 20-30 minutes to ensure the full extraction of active ingredients. Next, the mixture was heated over strong fire until boiling, maintained for 1-2 minutes, and then reduced to a gentle simmer over low heat for 20-30 minutes to ensure complete extraction of the active components. This decoction process was repeated three times, with the decoctions from all three cycles being combined. Afterward, the mixture was centrifuged at 3000 rpm for 15 minutes to remove any solid residues, and the supernatant was collected. Finally, the liquid was concentrated using a vacuum pump and rotary evaporator under conditions of 0.08 MPa and 60°C, until the concentration reached 1 g/mL, at which point the concentrated solution was set aside for future use. The medicine was provided by Xiangxiang Pharmacy, Guangxi Province, China. The positive control drug ribavirin was purchased from Solaiobao (Cat. No. R8370).

The CTA was identified by Panomik Biomedical Technology Co., Ltd. (Jiangsu, China). Sample preprocessing was carried out according to the relevant instructions (Vasilev et al., 2016). The raw data were first converted to mzXML using the MSConvert function in the ProteoWizard software package (v3.0.8789) (Rasmussen et al., 2022) and processed using R for identification (Navarro-Reig et al., 2015). Liquid chromatograph model Vanquish and mass spectrometer model Q Exactive, both purchased from Thermo, were used (Want et al., 2013; Zelena et al., 2009). The metabolites were identified by their accurate mass and MS/MS data, which were matched with various databases including HMDB (Wishart et al., 2007), massbank (Horai et al., 2010), LipidMaps (Sud et al., 2007), mzcloud (Abdelrazig et al., 2020), KEGG (Ogata et al., 1999), and the metabolite database built by Panomix Biomedical Tech Co., Ltd. (Suzhou, China). The molecular weight of metabolites was determined based on the mass-to-charge ratio of parent ions in the MS data. The molecular formula was predicted using adduct ions and then matched with the database for MS identification of metabolites. Additionally, the MS/MS data from the quantitative table of MS/MS data were matched with the fragment ions and other information of each metabolite in the database to achieve MS/MS identification of metabolites.

### In vitro experiments

**CTA cytotoxicity assay.** Precisely weigh the CTA sample to be tested and sterilize it in a 65°C water bath for 1 hour. After cooling the sample to room temperature, dilute it with DMEM (H) medium containing 2% fetal calf serum. Add antibiotics at a final concentration of 500 IU/mL and incubate at 4°C overnight. The experimental concentrations of the samples to be tested were: 200 mg/mL, 100 mg/mL, 50 mg/mL, 25 mg/mL, 12.5 mg/mL, and 6.25 mg/mL. Dilute CEK cells to a concentration of  $5 \times 10^4$  cells/mL, add 0.1 mL to each well of a 96-well cell plate, and culture them at 5% CO<sub>2</sub> and 37°C until the cell confluence reaches more than 80%. Then aspirate the culture medium from the wells to remove

the original culture medium. Add 100  $\mu$ L of culture medium containing the sample to be tested into each well. For each sample, set up six gradients, with each gradient containing six cell complex wells. A culture medium without the drug should be included as a normal cell control. After culturing for 60 hours, the OD value was measured at a wavelength of 450 nm using a microplate reader, following the instructions of CCK8. Finally, determine the half-toxic concentration corresponding to each tested sample using the Reed-Muench method.

**IBV replication experiments.** To determine viral replication, CEK cells were diluted to  $5 \times 10^4$  cells per mL and plated on a 24-well plate. When the cells reached 80% confluency, the culture medium was removed and the cells were washed three times with PBS. Subsequently, 0.4 mL of 100-fold diluted TCID<sub>50</sub> virus liquid was added to each well and incubated in a 37°C, 5% CO<sub>2</sub> incubator for 2 hours. After another round of PBS washing, a maintenance solution was added for continued culturing. At specific time points (6, 12, 18, 24, 30, 36, 42, 48, 54 and 60 hours), the cell plates were taken out and the cells in the corresponding wells were washed three times with PBS. Then, 20  $\mu$ L of BeyoDirect™ RNA Virus Direct RT-qPCR Preservation Solution (Cat. No. R0145-500mL) was added to each well, and the amount of viral mRNA was measured using a fluorescent quantitative RT-qPCR test. Each time point was repeated with 6 replicate wells, and 3 replicates were performed between the three groups. Fluorescent PCR determination of viral load in tracheal tissues and organs was conducted using primers and probes designed for the M41 strain (Accession No. FJ904720) as listed in Table 1. The primer and probe sequences were synthesized by Beijing Qingke Biotechnology Co., Ltd., and the fluorescent PCR premix enzyme (Cat. No. A039) from Bao Biotechnology Co., Ltd. was used. The total volume of the fluorescence quantitative PCR (probe method) was 20  $\mu$ L, and the reaction program consisted of: Premix Ex Taq™ (Perfect Real Time) 10  $\mu$ L, IBV-F (20 pmol/ $\mu$ L) and IBV-R (20 pmol/ $\mu$ L) 0.4  $\mu$ L each, IBV-P (20 pmol/ $\mu$ L) 0.3  $\mu$ L, template 2  $\mu$ L, and RNase-free Water 6.9  $\mu$ L. The amplification program included a pre-denaturation step at 95°C for 30 seconds, followed by denaturation at 95°C for 5 seconds, annealing at 62°C for 34 seconds for a total of 40 cycles, and fluorescence signals were collected simultaneously.

**Inhibition of CTA on the virus.** The CEK cells were diluted to a concentration of  $5 \times 10^4$  cells/mL and evenly distributed onto a 6-well culture plate. After the cells reached 80% confluency, the experiment was divided into three groups: 1) CTA First: drug administration followed by tapping group, which was first incubated with CTA-H, CTA-M, CTA-L solution (ribavirin as positive control, 10  $\mu$ g/mL (Chen, et al., 2019).) for 2 hours at 37°C, followed by the addition of 2 mL of medium containing viral solution, incubated at 37°C for 2 hours, discarding the viral solution, washed and then added with different concentrations of the drug solution (2 mL per well). The incubation was continued for 48 hours. 2) CTA Simultaneously: For CTA first, 2 mL of virus-containing medium was added, incubated at 37°C for 2 hours, discarded the virus solution, washed, and then drug solution (2 mL per well) was added, and the incubation was continued for 48 hours. 3) CTA Later: For CTA simultaneous, virus-containing medium was added, drug solution (2 mL per well) was added, incubated at 37°C for 2 hours, and then washed, and then drug solution (2 mL per well) was added, and the incubation was continued for 48 hours. and incubated at 37°C for 2 hours, discarded the medium and continued incubation for 48 hours. All groups were

washed 3 times with PBS at the end of incubation, and the amount of viral mRNA in CEK cells was detected by fluorescence quantitative PCR.

**Tracheal ring experiment.** Aseptically remove the trachea from a 20-day-old SPF chicken embryo, ensuring the removal of surrounding connective tissue and fat. Rinse the trachea with PBS and use ophthalmic scissors to cut it into approximately 1 mm thick tracheal rings. Place the tracheal rings in a 24-well plate, with each well containing 3 rings. Utilize an inverted microscope to observe and select tracheal rings with active ciliary movement for subsequent experiments. The grouping of this experiment and the dosage of drugs used in each group were referred to the results of CCK8 experiment of CTA. Viral solution was added to the cell wells containing tracheal rings at 0.5 mL per well and incubated continuously at 37°C for 48 hours. Negative control wells only receive nutrient solution, while positive wells receive virus dilution. Additionally, the experiment includes experimental groups where the viral challenge is administered before the drug, as well as simultaneous administration of the drug and challenge. Based on the experimental results, calculate the protection rate using the formula: the number of tracheal rings with ciliary movement divided by the total number of tracheal rings, multiplied by 100%.

**Chicken embryo experiment.** For this study, 9-day-old SPF eggs were obtained from the Guangxi Veterinary Research Institute. The eggs were incubated at 37.5°C for 24 hours to acclimate and their viability was checked using a flashlight. Chicken embryos at 10 days old were then exposed to a challenge dose of 100 times the median EID<sub>50</sub>, followed by treatment with the same dose of traditional Chinese medicine after 3 hours. The specific experimental operation is: with a 1 mL syringe to draw up the appropriate amount of viral allantoic fluid or drug, chicken embryo air chamber end well sterilised after using a torch light to find a suitable injection point avoiding the blood vessels, syringe needle all the way into the egg, slowly in the chorionic allantoic membrane to release the liquid. The injection port on the surface of the egg was then closed using liquid paraffin and examined by light after 24 hours. The blank group received the same dose of normal saline. The research design consisted of 7 groups: NC, NC-CTA (M), CTA-H, CTA-M, CTA-L, Ribavirin (100mg/mL), and IBV. Based on relevant studies, Ribavirin was selected as the positive control drug, and the doses used *in vivo* and *in vitro* were referred to relevant studies (Chen, Muhammad, Zhang, Ren, Zhang, Huang, Diao, Liu, Li, Sun, Abbas and Li, 2019b). Traditional Chinese medicines are used within safe and reasonable dosages. Each group had 10 chicken embryos, with 0.1 mL of medicine or saline added to each embryo. The experiment was repeated three times. IBV infection in the embryos was determined by observing characteristic embryonic lesions such as developmental delay, curling, and embryonic clubbing. The eggs in each group were observed twice a day under a candle, and any eggs with dead embryos were transferred to the refrigerator. After 7 days of observation, the embryos were assessed for signs of health, including the number and size of chorioallantoic membrane veins and the movement of the embryos, compared to the control group. At the end of the experiment, all eggs in each group were individually weighed. The embryos were then removed washed and weighed again. The embryonic index (EI) of all eggs was calculated using the formula: EI = (Embryo weight (g) / Egg weight (g))  $\times$  10000 (Dhinakar Raj et al., 2004).

#### Animal experiment

**In Vivo Experimental Design.** A total of 140 Sanyellow chickens were selected for this experiment from Guangxi Fufeng Agriculture and Animal Husbandry Group Co., Ltd. (Nanning, China). The chicks were kept in well-ventilated wire cages with a relative humidity maintained between 50% and 55%. The lighting schedule was set at 24 hours from 1 to 14 days of age, gradually reducing to 20 hours. The cage temperature was maintained between 32°C and 34°C from 1 to 7 days of age and then gradually decreased to 26°C. Throughout the experiment, the chickens had free access to food and water. The experimental chickens were divided into 7 groups according to their body weight measured at 14

**Table 1**  
Design of the IBV primer probe.

Primer	Primer sequences(5' to 3')	base number	temperature
IBV-F	5'-TTGAAGGTAGYGGYGTTCCTGA-3'	22bp	60°C
IBV-R	5'-CAGMAACCCACACATATACCATC-3'	22bp	60°C
IBV-P	FAM- ACTGGAACAGGACCGCGTGAACCT- BHQ1	26bp	60°C

days of age, with 20 chickens in each group. The groups included the blank group (NC), blank medication group (NC-CTA, 2 mL/0.5 L), high-dose medication group (CTA-H, 4 mL/0.5 L), medium-dose medication group (CTA-M, 2 mL/0.5 L), low-dose medication group (CTA-L, 1 mL/0.5 L), positive drug group (Ribavirin, 100 mg/0.5 L), and model group (IBV). Ribavirin doses used were referred to relevant studies(Chen et al., 2019b). Traditional Chinese medicines are used within safe and reasonable dosages. The blank group and IBV group served as control groups and were administered with physiological saline. The drug groups were fed continuously for 1 week starting from the 14th day of the experiment, and the entire experiment lasted for 21 days. On the day of the challenge, CTA was administered to all groups except the blank control group. The chickens in the other groups were attacked by 105 times EID<sub>50</sub> on the nose-eye route. All birds were housed in molded plastic breakaway isolators and provided with free feed. The animal experiment was conducted following the guidelines of the Animal Protection and Welfare Committee of Guangxi University (Approval Number: GXU-2023-0178), ensuring strict adherence to animal ethics.

**Efficacy evaluation.** The drug was administered continuously for 7 days and then stopped for 7 days (14dpi). During the period from 3dpi to 14dpi, the clinical efficacy of the last group of test chickens (5 chickens) was evaluated according to the chick clinical symptom scoring standards in Table 2.

**Growth performance and immune organ index.** At 3dpi, 7dpi, and 14dpi, the average body weight, average weight gain, and average weight gain rate of each test group were calculated by repeatedly weighing 5 chickens from each group. The average daily weight gain (g/d feather) was calculated using the formula: (last weight - starting weight) / number of feeding days/feather. The spleen, thymus, and bursa of Fabricius of five chickens in each group were collected and weighed, and the relative organ weight was calculated to express the immune organ index. The organ index was calculated as organ weight (mg) / body weight (g).

**Viral load detection based on qPCR.** At 3dpi, 7dpi, and 14dpi, 5 chickens in each group were randomly selected and euthanized by cervical dislocation. Tracheal and sinus swab samples were collected for viral load detection. The column viral DNA/RNA extraction kit (Genstar, Cat. No. P142-01) was used for nucleic acid extraction, and the reverse transcription kit (Genstar, Cat. No. A232-02) was used to reverse-transcribe the viral RNA into cDNA. The viral load was detected using the previous experimental method for qPCR viral load detection.

**Detection of specific anti-IBV antibodies.** The serum of 5 chickens from each group was collected at 3dpi, 7dpi, and 14dpi. An indirect enzyme-linked immunosorbent assay (ELISA) kit provided by Biolab

(Cat. No. FZ067) was used, following the manufacturer’s instructions, to test for total serum IBV-specific antibodies.

**Blood routine and cytokine detection.** On the 7th day after infection (7dpi), blood samples were collected from 5 chickens in each group and placed in sodium citrate anticoagulant tubes. The Mindray BC5000 hematology meter was used to measure various parameters including white blood cell count (WBC), red blood cell count (RBC), hemoglobin (HGB), hematocrit (HTC), mean corpuscular hemoglobin concentration (MCHC), platelet hematocrit (PLT), platelet count (PCT), and neutrophil percentage (GRAN%). Additionally, serum samples from 5 chickens in each group were collected on the 7th day after infection (7dpi). The inflammatory factors IL-4, TNF- $\alpha$ , IFN- $\gamma$ , IL-10, IL-6, and IL-1 $\beta$  were detected using the ELISA kit from Boyan (Nanjing, China) as per the provided instructions. Oxidative stress was evaluated using nitric oxide (NO) trace biochemical kits from Boyan (Nanjing, China) and total antioxidant capacity (T-AOC), superoxide dismutase (SOD), malondialdehyde (MDA), and xanthine oxidase (XOD) trace biochemical kits from Soleba (China). The Mindray BS-2000M fully automatic biochemical analyzer was used to measure various indicators including total bilirubin (TBIL), direct bilirubin (DBIL), total protein (TP), albumin (ALB), globulin (GLB),  $\gamma$ -glutamyl transpeptidase ( $\gamma$ -GT), alanine aminotransferase (ALT), aspartate aminotransferase (AST), alkaline phosphatase (ALP), lactate dehydrogenase (LDH), urea (Urea), uric acid (UA), superoxide dismutase (SOD), total cholesterol (TC), triglyceride (TG), and glucose (GLU).

**Pathology of trachea and lung.** The trachea and lung tissues were fixed by 4% paraformaldehyde in a good state of fixation, then trimmed, dehydrated, embedded, sectioned, stained, sealed and finally microscopically examined for qualified samples. Browse the sections under the microscope or browse the digital sections, observe the tissue sections in detail at different magnifications, describe the basic pathological changes in the sections such as congestion, bruising, haemorrhage, oedema, degeneration, necrosis, proliferation, fibrosis, mechanisation, granulation tissue, inflammatory changes in text, and reflect the differences between the slices. Image acquisition instruments: orthogonal white light photographic microscope, Nikon (Japan), Eclipse Ci-L.

*Joint analysis of non-targeted metabolomics and network pharmacology*

**Non-targeted metabolomics analysis and identification of blood components.** Serum samples from three chickens each from the NC group, IBV group, and CTA-M group at 7 dpi were collected for non-targeted metabolomic analysis. LC-MS was used to detect the chicken serum using the CTA component identification method and matched it with the database. Two different multivariate statistical analysis models, unsupervised and supervised, were applied using the R ropls (v1.22.0) package to discriminate between the groups(Thevenot et al., 2015). The statistical significance of the P-value was determined by conducting a statistical test between the groups. Biomarker metabolites were selected based on a combination of the P-value, VIP (OPLS-DA variable projection importance), and FC (multiple of the difference between groups). Metabolites with a P-value of 1 were considered to have significant differential expression. Pathway analysis of the differential metabolites was performed using MetaboAnalyst(Xia and Wishart, 2011). The identified metabolites in metabolomics were then mapped to the KEGG pathway for biological interpretation of higher-level systemic functions. The metabolites and corresponding pathways were visualized using the KEGG Mapper tool.

**Network Pharmacological analysis.** The analysis object of network pharmacology in this study focused on the effective blood components of CTA in non-targeted metabolomics. To identify potential targets, the researchers utilized the Swiss Target Prediction Server and the needle and thread tool for chemical interaction analysis. Additionally, the study employed the Gene Cards and OMIM databases to identify disease targets associated with the 'Infectious Bronchitis Virus' (IBV). The genes identified from both databases were merged, eliminating duplicates, and

**Table 2**  
Chick clinical symptom scoring criteria.

Curative effect	Clinical symptom	Value
death	The dead chickens were found to have died of infectious bronchitis after necropsy and PCR testing.	5
invalid	Chickens may exhibit symptoms of depression such as lying down, rough feathers, closed eyes, lethargy, reduced food consumption, neck stretching, severe rales, visible mucus in the mouth and nose, coughing, and white or watery diarrhea.	4
Somewhat relieved	The chicken displays signs of low energy, reluctance to exercise, decreased appetite, a slight cough, abnormal breath sounds (rales), presence of mucus in the mouth and nasal cavity, and mild diarrhea.	3
moderately relieved	The chicken is in a good mental state, occasionally exercises, has a decreased appetite, breathes through the mouth, and has mucus in the mouth.	2
considerably relieved	The chickens exhibit signs of good mental well-being, with normal breathing and appetite. Some chickens may display mouth breathing and have a slight presence of mucus in their mouths.	1
completely relieved	The chicken is in good spirits and its breathing and appetite have returned to normal.	0



resulting in a comprehensive list of IBV-related targets. To identify common targets between CTA and IBV, the researchers utilized Venny 2.1 software. Furthermore, a visual network diagram illustrating the relationship between the active ingredients of CTA, its targets, and IBV targets was constructed using Cytoscape\_3.8.0 software. For protein interaction information related to cross-targets, the String database was utilized, with the species set to 'Gallus' and a confidence level above 0.04 selected. This approach facilitated the identification of key target proteins, providing valuable insights. The effect of CTA on key target proteins associated with IBV was analyzed using the cluster analyzer package in R software, with a corrected *P*-value less than 0.05 as the screening criterion (last update: December 20, 2023)(Luo and Brouwer, 2013). GO analysis and KEGG analysis were performed on the CTA anti-IBV targets. The relevant files were exported, and the number of targets was arranged in descending order. The top 10 targets in each of the three branch targets of GO were ranked, and a GO circle diagram was generated. The top 10 ranked genes were evaluated using Bioconductor and the Hubba gene module in Cytoscape\_v3.7.1 software to create a Sankey diagram(Peng et al., 2022b).

**Joint analysis utilizes.** The screening of key metabolic pathways in non-targeted metabolomics was conducted using a *P*-value  $\leq 0.05$  criterion. Relevant metabolites were identified through metabolic pathways, and related targets were predicted using the Swiss Target Prediction Server. Additionally, by analyzing traditional Chinese medicine components and blood components, we obtained compounds associated with key metabolic pathways. The relevant targets predicted by non-targeted metabolomics were intersected with the main targets of network pharmacology, and key targets were identified using eight algorithms from the cytohubba plugin (MCC, MNC, Degree, BottleNeck, Closeness, Radiality, Betweenness, and Stress). The effector substances related to these targets were determined based on the analysis results from swiss target prediction. Structural processing of the compound (ligand) and target protein (receptor) was performed using the Yinfu Cloud platform, followed by molecular docking through Discover to identify the best docking site for docking binding mode analysis. The molecules' docking status was visualized using PyMol software.

**Target validation.** At 7dpi, five chickens from each group were selected and sacrificed. The tracheas were collected and the expression levels of STAT3, EGFR, CDK2, and FOXO genes were verified using RT-qPCR. The Beyotime RNA/Protein Co-extraction Kit (Cat. No. R0018M) was used to extract RNA and protein according to the manufacturer's instructions. RNA was dissolved in the water phase and purified by precipitating it with isopropanol. DNA was precipitated with absolute ethanol from the middle phase and the lower red organic phase, and the organic phase was further precipitated with isopropanol to obtain purified protein. The isolated RNA samples were reverse transcribed into cDNA using StarScript III All-in-one RT Mix with gDNA Remover Reverse Transcription (GenStar, China). Subsequently, cDNA and primers were combined in the 2x Realstar Green Fast Mixture system (GenStar, China) following the manufacturer's instructions to conduct real-time RT-qPCR. Internal reference genes were utilized for normalizing the expression of target genes. Primer sequences for RT-qPCR can

**Table 3**  
Primers and probes used for amplifying SAT3A, CDK2 and EGFR.

Gene	Primer and probe Sequence (5'-3')	Temperatures	GenBank
STATA3	F: GTGCTGCTCGGTATCTGAAG R: TCTGCTCCCTCGCTACTGTT	55°C	NM_001030931.4
CDK2	F: CCAGAACCTCCTCATCAAC R: CAGATGTCCACAGCAGTC	55°C	NM_001199857.2
EGFR	F: CTGCCATCCAACTGTACACGA R: GACCGATGCCTAGACCAACCA	60°C	NM_205497
B-actin	F: CTGGCACCTAGCACAAATGAA	60°C	NM_205518.1

be found in Table 3. All primers underwent specificity testing, and experimental procedures were carried out as per the manufacturer's guidelines with modifications based on the annealing temperatures provided in the table. Each RT-qPCR analysis was replicated three times to assess the expression levels of candidate genes. Three samples from each group were randomly selected, and the extracted proteins were mixed with loading buffer, boiled in water for 10 minutes, separated using SDS-PAGE, and transferred to a PEDV membrane. Following the transfer, the membrane was blocked and washed thrice with PBST. Subsequently, the primary antibody specific (STAT3 Cat. #TA6294S, CDK2 Cat. #PA1205S, EGFR Cat. #TA6042S, FOXO3a Cat. #TA6020S, pFOXO3a Cat. #TA7124S, Abmart, China) to the target gene was incubated overnight at 4°C, followed by three washes with PBST. The membrane was then exposed to Goat Anti-Rabbit Mouse IgG-HRP(Cat. #M21003, Abmart, China). The bound proteins were identified using an ECL kit (Genstar, China).

Statistical analysis

Replicates (n = 5) were treated as one experimental unit. Statistical analysis of all data was performed using GraphPad Prism 9 and WPS Excel. GraphPad Prism 9 was used to obtain clinical sign score curves. For the statistical analysis of viral load, organ index, IBV-specific antibody titer, blood routine, and serum cytokine concentration, qPCR was conducted using one-way analysis of variance (ANOVA) with Prism 9 software. Post hoc analysis was performed using Tukey's test to determine significant differences between treatments. *P*-values less than 0.05 (*p* < 0.05) were considered significant, and those less than 0.01 were considered highly significant.

Results

Preparation of compound throat anti-viral

A total of 353 prescriptions were screened for treating cough, involving 361 types of drugs. A database was constructed specifically for treating chicken infectious bronchitis. Table 4 provides a summary of

**Table 4**  
Drugs with a frequency greater than 25 in traditional Chinese medicine prescriptions.

Number	Medicinal materials	frequency
1	licorice	179
2	Platycodon	139
3	bitter almond	135
4	Fritillaria fritillary	125
5	Ephedra	114
6	Pinellia ternata	100
7	tangerine peel	98
8	perilla	87
9	skullcap.	79
10	Stemona japonica	78
11	Mentha canadensis	72
12	Morus alba	68
13	plaster	67
14	Peucedanum praeruptorum	62
15	Eriobotrya japonica	61
16	Ophiopogon japonicus	49
17	Wolfiporia extensa	48
18	Tussilago farfara	48
19	Schisandra chinensis	45
21	Anemarrhena asphodeloides	39
22	Vincetoxicum glaucescens	31
23	Papaver somniferum	30
24	Trichosanthes uniflora	28
25	Draba nemorosa	27
26	borneol	27
27	Citrus aurantium var. decumana	26
28	Rehmannia glutinosa	25

the analysis of the frequency of the 361 included traditional Chinese medicines, referred to as 'drug frequency'. The analysis reveals that the total frequency of medicines is 2,087, with 28 types of traditional Chinese medicines having frequencies greater than 25. Furthermore, a cluster analysis was conducted on the 353 first prescriptions and the 361 traditional Chinese medicines, resulting in the generation of 1 CTA. The recommended proportion of ingredients for CTA is as follows: *Rehmannia glutinosa* (18%), *Fritillaria fritillaris* (18%), *Ophiopogon japonicus* (18%), *Licorice* (14%), *Borneol* (14%), and *Bitter almond* (18%). The complex was prepared into a 500 mL, 1 g/mL aqueous extract for component identification. Fig. 1A depicts a chromatogram of the extract. In this test, a total of 484 metabolites were identified, including succinic acid semialdehyde, L-glutamine, and 2-oxoarginine. These metabolites include 67 carboxylic acids and derivatives, 45 benzene and substituted derivatives, and 43 fatty acyls, as well as 329 other compounds (Supplementary Materials 1, Fig. 1B).

### *In vitro* efficacy experiment of CTA

**Antiviral effect of CTA on CEK.** When conducting the CCK8 cytotoxicity assay, various concentrations of CTA were utilized. The results indicated that there was no significant difference ( $P > 0.05$ ) between the drug group and the blank control group when the CTA concentration reached 25 mg/mL. However, a significant difference was observed between the drug group and the blank group at a CTA concentration of 50 mg/mL. Consequently, a concentration of 12.5 mg/mL CTA-M was chosen for subsequent experiments (Fig. 2A). In this experiment, the high and low concentrations of the drug were 25 mg/mL and 6.25 mg/mL, respectively. Ribavirin (10 µg/mL) was used as a reference. TCID<sub>50</sub> was determined using the Reed-Muench method, yielding a result of  $10^{-5.16}$ /1mL. Stable typical cytopathic effects (CPE) were observed 36 hours after IBV infection. The results of the viral proliferation curve demonstrated that IBV was capable of infecting and replicating in CEK cells, reaching a TCID per 100 µl 36 hours after inoculation (Fig. 2B). RT-qPCR was employed to assess the antiviral effect of CTA by detecting the relative expression level of IBV-N gene mRNA (Fig. 2C). At the maximum non-toxic concentration of the drug, CTA's inhibitory effect on IBV was comparable to or even surpassed that of ribavirin. In the experiment involving first administration and then challenge, the virus inhibition rate was higher compared to the other two experimental modes. Additionally, the dosage of CTA on cells exhibited a dose-dependent relationship, with significant differences observed between all medication groups and the IBV group (Fig. 2E). Thus, it can be concluded that CTA possesses an *in vitro* antiviral effect, similar to that of Western medicine.

**Tracheal ring experiment.** The experiment evaluated the effects of treating CTA and IBV at 100 times TCID<sub>50</sub> on the embryonic trachea, within the safe concentration range of the reference drug. At 48 hours after inoculating with IBV M41 virulent strain, noticeable differences were observed between the experimental group and the positive vaccination group. Throughout the entire test period, the tracheal rings of the blank medication group and the medication group showed attached and active cilia, with a relatively clean ring and no shedding of tracheal epithelial cells. In the positive viral challenge group, the ciliary

movement of the tracheal ring ceased, secretions increased, and a significant number of epithelial cells shrank and detached. The majority of tracheal ring cilia in the CTA-H group remained active, while the movement of tracheal ring cilia in the CTA-M group was also significantly better than that in the positive viral challenge group. By seventy-two hours after viral challenge, in both the ribavirin group and the CTA-L group, the majority of tracheal ring movements in the positive viral challenge group had stopped. The ribavirin group showed a higher rate of tracheal ring protection against IBV infection compared to the CTA-L group. This trend was consistent regardless of the order of challenge administration (Table 5). These findings demonstrate that within a certain concentration range, the treatment can effectively prevent and reduce tracheal ring lesions and inhibit virus-infected cells.

**Chicken embryo experiment.** In this study, 10-day-old chicken embryos were injected with IBV and incubated for 5 days. The embryos were then dissected to assess the extent of the lesions. The EID<sub>50</sub> was calculated using the Reed-Muench method, and the result was determined to be  $10^{-6.16}$ /1mL. Subsequently, chicken embryos were injected with a dose of 100 times EID<sub>50</sub> of the IBV M41 strain and administered 2 hours later. The results revealed that EI of the IBV group was  $997.600 \pm 344.746$ , and all embryos died at the end of the experiment. In contrast, the control group, which did not receive IBV-M41 injection, had a 100% survival rate and an EI of  $3761.21 \pm 132.501$  (Fig. 2D). It is important to note that chicken embryos that died within 24 hours were excluded from the experiment, indicating that IBV-M41 injection was the sole cause of the significant decrease in EI. The results of the NC-CTA group were similar to those of the NC group. Furthermore, the treatment group exhibited a significant increase in EI compared to the IBV group. Although the CTA medication group showed some dose dependence, it was not pronounced, and its efficacy was significantly better than that of the ribavirin group. These findings suggest that CTA-L has the least toxicity to chicken embryos, reduces mortality, and improves dysplasia. Therefore, CTA is deemed an effective drug for the treatment of IBV M41 virus-infected chick embryos.

### *In vivo* efficacy test of CTA

**Analysis of clinical signs of CTA.** Clinical signs of IBV infection in chicks were observed and evaluated at different time intervals (Fig. 3A). On the 3rd day after the challenge, the chicks exhibited symptoms such as continuous depression, decreased appetite, increased water consumption, frequent head shaking, drooping wings, coughing, mouth breathing, and tracheal rales. Throughout the observation period, the symptom scores of the ribavirin group and IBV group consistently remained higher, while the CTA-H group had the lowest symptom score after medication, and the CTA-M group's score was almost equivalent to the CTA-H group. By day 14, the symptom scores of all chickens in the CTA-H and CTA-M groups dropped to 0, while more than half of the chickens in the virus group were still ill, although their scores were the same as those of the CTA-L group. The CTA-H group demonstrated better treatment efficacy throughout the observation period. On the 14th day, the CTA-H group exhibited the highest weight gain rate, and the average final weight was similar to that of the blank control group. The CTA-M group and NC-CTA group also showed similar results to the blank group,

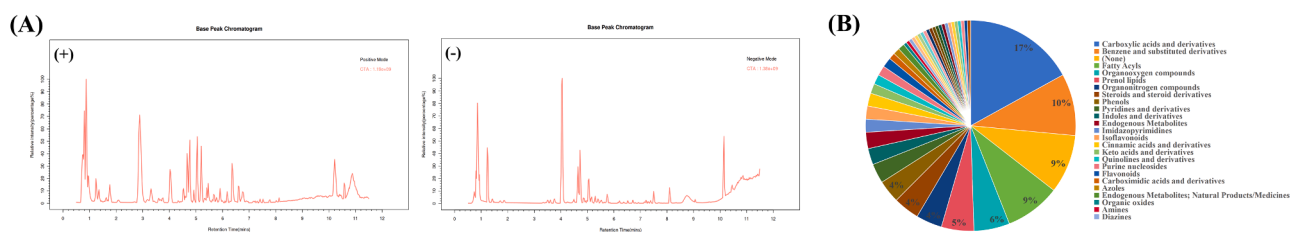
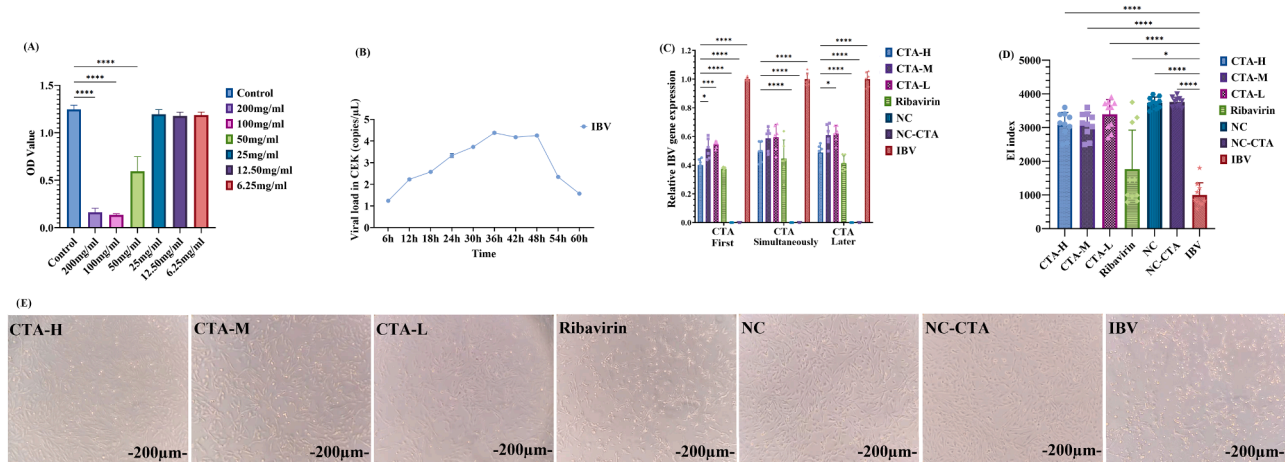


Fig. 1. A: Positive ion diagram, B: Negative ion diagram. The abscissa is the retention time, the ordinate is the ion intensity, and the upper right corner of the diagram represents the maximum ion intensity of each sample. Different colors represent different groups.



**Fig. 2.** (A) Toxicity test of CTA on CEK cells. The data are expressed as mean  $\pm$  SD,  $n = 6$ ; (B) IBV replication experiment on CEK cells; (C) Inhibitory effect of CTA on viruses. The data are expressed as mean  $\pm$  SD,  $n = 6$ ; (D) Antiviral EI index determination of CTA on chicken embryos. The data are expressed as mean  $\pm$  SD,  $n = 10$ ; (E) Changes in CEK cell morphology in different treatment groups. Statistical significance is indicated by \*  $p < 0.05$ , \*\*  $p < 0.01$ , \*\*\*  $p < 0.001$ .

**Table 5**  
Tracheal ring protection rate experiment.

Group	Before	Together	After
CTA-H	77.78%	77.78%	88.89%
CTA-M	66.67%	77.78%	100.00%
CTA-L	55.56%	44.44%	44.44%
Ribavirin	77.78%	66.67%	55.56%
NC	100	100	100
NC-CTA	100	100	100
IBV	0	0	0

while the chicks' weight gain rate in the ribavirin group was lower than that of the challenge group and other medication groups. There was a significant difference in the weight gain index between each group, indicating that CTA had a substantial effect on improving the decline in chick production performance caused by IBV, whereas the western medicine ribavirin had no therapeutic effect on the decline in chick production performance (Fig. 3B). Compared with the blank group and virus model group, there was no significant difference in Thymus and Bursa of Fabricius after CTA treatment, especially in the CTA-H group, although ribavirin was more effective in stimulating the exponential increase in immune organs (Fig. 3C).

**Anti-IBV effect of CTA.** To evaluate the inhibitory effect of CTA, the study conducted qPCR to measure viral mRNA levels in the trachea and lungs of different groups at 3dpi, 7dpi, and 14dpi. No virus was detected in the trachea and lungs of the chickens in the two control groups. Overall, the expression level of IBV mRNA in the trachea of the challenge control group was significantly higher than that of the positive drug

group and CTA group. Additionally, CTA consistently reduced the level of viral mRNA compared to the challenge control group. At 3dpi, both CTA-H and CTA-M significantly inhibited virus replication in the trachea compared to the challenge control group. CTA-M also exhibited a lower viral load in the trachea compared to the challenge control group. However, there was little difference in the therapeutic effect of several drugs on the trachea of chicks at 7dpi and 14dpi (Fig. 4A). At 7dpi, due to the use of a drug treatment that prevented further spread of the virus in the lungs, some samples showed viral load values of 0, resulting in long error bars for five samples. At 14 dpi, both the mid-dose and high-dose CTA groups successfully cleared the virus from the lungs (Fig. 4B).

To test the adjuvant effect of CTA on the humoral immune response of birds, blood samples were collected from the subwing veins of 5 chickens in each group at 3dpi, 7dpi, and 14dpi. The antibody titers were determined by ELISA, and samples with titers less than 0.3 were considered negative for anti-IBV antibodies (Fig. 4C). After the challenge, the antibody titers significantly increased in both the challenge control group and the drug group. At 3dpi and 7dpi, the chickens in the challenge control group had higher antibody titers compared to the chickens in the blank control group. At 7dpi, the CTA-H group exhibited the highest antibody titer among all the groups. Furthermore, at 14dpi, the CTA-M group showed higher antibody levels than the other groups, and the OD<sub>450</sub> values of all samples were greater than 0.3, indicating that the sera of these five chickens had converted to anti-IBV antibody positivity within 14 days. No clear dose dependence was observed during the experiment, suggesting that CTA can enhance the humoral immune response.

**Effects of CTA on blood routine, serum biochemistry and cytokines.** The results in Table 6 indicate that there are no significant differences in

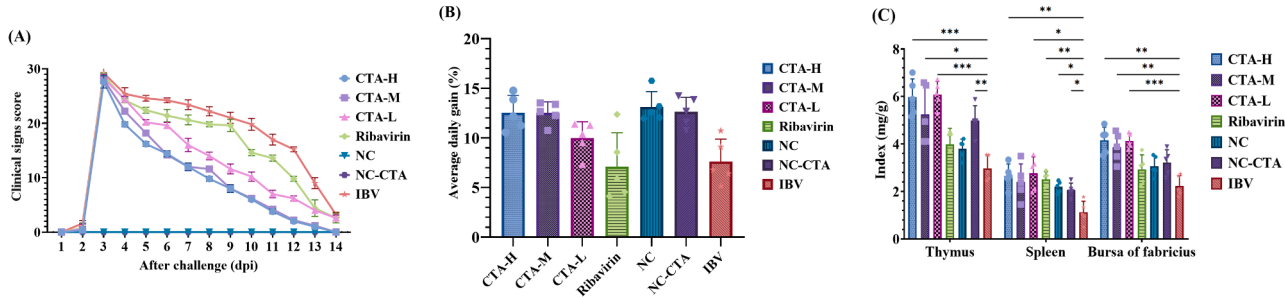


**Fig. 3.** (A) Clinical sign scores of IBV-infected chicks treated with CTA at different periods; (B) Effect of CTA on production performance of chicks at 14dpi; (C) Effect of CTA on organ index of chicks at 7dpi. The data are expressed as mean  $\pm$  SD,  $n = 6$ . Compared with IBV group, significance of differences is marked as \*  $p < 0.05$ , \*\*  $p < 0.01$ , \*\*\*  $p < 0.001$ .

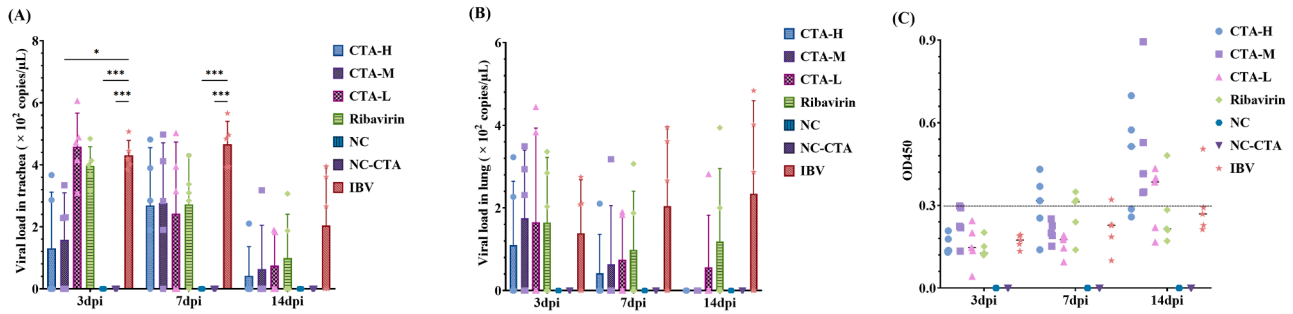


**Fig. 4.** (A&B) Virus loading in the trachea (A), and lungs (B).IBV RNA levels in trachea and lungs were assessed at 3dpi, 7dpi and 14dpi; (C) IBV-induced antibodies. In order to detect the effect of CTA on the immune response of chicks infected with IBV, the serum of 5 chickens in each group was collected at 3dpi, 7dpi and 14dpi for antibody detection. Samples with an OD<sub>450</sub> value less than 0.3 were considered negative for anti-IBV antibodies. The data are expressed as mean  $\pm$  SD, n = 5; compared with IBV group, significance of differences is marked as \*  $p < 0.05$ , \*\*  $p < 0.01$ , \*\*\*  $p < 0.001$ .

WBC and MCHC among different blood routine samples at 7dpi. CTA-M has a certain impact on the three hematological indicators of chicken RBC, PLT, and GRAN%. In comparison to the IBV group, the NC group exhibited significant or extremely significant differences in 6 indicators: RBC, HGB, HTC, PLT, PCT, and GRAN%. Similarly, the NC-CTA group showed significant or extremely significant differences in the four indicators of HTC, PLT, PCT, and GRAN% when compared to the IBV group.

After administering CTA to the target animal for 7 days, we measured its serum biochemical indicators and recorded the results in Table 7. The table reveals that, apart from  $\gamma$ -GT, LDH, Urea, UA, and GLU, the CTA-M group exhibited significant or extremely significant differences compared to the IBV group in terms of other indicators. Furthermore, there were also variations in certain indicators between the other two CTA treatment groups and both the ribavirin group and the IBV group. In conclusion, the experimental findings demonstrate that the CTA-M group had a more pronounced overall impact on the chicken's serum biochemical indicators.

This study investigated the impact of CTA on oxidative stress markers in chickens infected with IBV. The markers examined were MDA, SOD, T-AOC, XOD, and NO. Fig. 5A demonstrates that following IBV infection, the experimental group displayed significantly lower levels of T-AOC and NO compared to the NC group and NC-CTA group. Conversely, the XOD and MDA levels decreased in the experimental group after IBV infection in comparison to the uninfected group. The SOD group exhibited no significant differences throughout the detection process. Following CTA treatment, the levels of oxidative factors gradually approached those of the NC group. In conclusion, the CTA-H group outperformed in all five antioxidant indicators.

This experiment investigated the impact of CTA on the inflammatory response of chickens infected with IBV (Fig. 5B). Comparing the non-challenged group with the IBV-affected group, there was a decrease in IL-4, IFN- $\gamma$ , and IL-10 production, while TNF- $\alpha$ , IL-6, and IL-1 $\beta$

production increased. Comparing the IBV group with CTA-H and CTA-M, there were significant or extremely significant differences in IL-4, TNF- $\alpha$ , IFN- $\gamma$ , and IL-10 indicators, and they tended to be similar to those of the blank group. There was a highly significant difference in IL-1 $\beta$  between CTA-M and IBV groups. However, no significant differences were observed in IL-6 between all drug treatment groups compared to the IBV group. Overall, the CTA-M group exhibited a better anti-inflammatory effect.

CTA treatment could alleviate the IBV-induced clinical symptoms and pathological damage. According to the histopathological results at 7 dpi (Fig. 6), the trachea of the IBV group exhibited severe damage. Histological changes included the loss of tracheal cilia and the infiltration of a large number of inflammatory cells in the submucosa, with mononuclear cell and lymphocyte infiltration mainly occurring in the submucosa. The degree of organ damage in the ribavirin group did not significantly differ from that in the IBV group. However, the tracheal lesions in the CTA group were milder compared to the IBV group, and the CTA-M group showed the mildest pathological changes, characterized by mild ciliary loss, glandular degeneration, and congestion. Notably, the mucosa exhibited a more prominent loss of cilia, glandular degeneration, and infiltration of mononuclear cells and lymphocytes. The qPCR results revealed severe parabronchial and vascular hemorrhage in lung pathology sections of the IBV-affected samples. The alveolar spaces of the CTA-treated group showed a small amount of monocyte and lymphocyte infiltration, while the chicks in the CTA-M group exhibited only slight infiltration of monocytes and lymphocytes.

#### Joint analysis of non-targeted metabolomics and network pharmacology

**Non-targeted metabolomics analysis and identification of blood components.** In the experiment, chick serum at 7 dpi was utilized for non-targeted metabolomics experimental verification. The serum sample underwent chromatographic separation and entered the mass

**Table 6**  
Effects of CTA on routine blood test of chickens.

Index	CTA-H	CTA-M	CTA-L	Ribavirin	NC	NC-CTA	IBV
WBC	187.14 $\pm$ 9.80	185.56 $\pm$ 7.22	179.72 $\pm$ 8.78	192.60 $\pm$ 8.69	189.02 $\pm$ 3.62	189.62 $\pm$ 2.92	187.46 $\pm$ 8.72
RBC	3.00 $\pm$ 0.24	2.85 $\pm$ 0.14*	3.04 $\pm$ 0.18	3.33 $\pm$ 0.18	2.87 $\pm$ 0.14*	2.96 $\pm$ 0.18	3.22 $\pm$ 0.13
HGB	85.40 $\pm$ 6.66	79.20 $\pm$ 11.26	81.60 $\pm$ 10.43	105.60 $\pm$ 9.29	72.80 $\pm$ 6.83*	75.60 $\pm$ 8.91	104.60 $\pm$ 17.24
HTC	28.94 $\pm$ 3.64	29.60 $\pm$ 3.20	30.04 $\pm$ 1.72	34.84 $\pm$ 3.44	23.82 $\pm$ 2.19*	23.74 $\pm$ 0.66*	33.00 $\pm$ 4.55
MCHC	331.80 $\pm$ 2.68	322.60 $\pm$ 8.79	314.20 $\pm$ 11.69	337.60 $\pm$ 11.28	308.40 $\pm$ 7.16	315.20 $\pm$ 5.63	314.80 $\pm$ 13.08
PLT	40.20 $\pm$ 17.21	57.00 $\pm$ 2.55*	35.80 $\pm$ 9.31	43.60 $\pm$ 24.34	67.20 $\pm$ 4.55**	60.6 $\pm$ 2.07*	36.60 $\pm$ 10.26
PCT	0.03 $\pm$ 0.01	0.04 $\pm$ 0.01	0.02 $\pm$ 0.01	0.02 $\pm$ 0.02	0.06 $\pm$ 0.01*	0.06 $\pm$ 0.01*	0.03 $\pm$ 0.01
GRAN%	13.27 $\pm$ 2.02	11.73 $\pm$ 1.35*	14.99 $\pm$ 1.21	14.42 $\pm$ 1.47	9.68 $\pm$ 0.24***	10.11 $\pm$ 0.64***	14.39 $\pm$ 0.83

The data are expressed as mean  $\pm$  SD, n = 5; compared with IBV group, significance of differences is marked as

\*  $p < 0.05$

\*\*  $p < 0.01$

\*\*\*  $p < 0.001$ .



**Table 7**  
Effects of CTA on serum biochemistry of chickens.

Index	CTA-H	CTA-M	CTA-L	Ribavirin	NC	NC-CTA	IBV
TBIL	13.83±1.86	18.59±1.37**	14.66±1.03	14.77±0.72	19.76±2.91*	15.23±2.30	13.76±1.68
DBIL	0.54±0.15	0.73±0.10*	0.67±0.06	0.56±0.07	0.85±0.25	0.59±0.21	0.53±0.09
TP	31.73±5.56	21.75±1.67***	27.43±1.61	28.12±0.94	20.41±1.34***	20.10±1.32***	29.02±1.13
ALB	10.70±4.00	7.78±1.58*	9.00±1.17*	9.4±0.62*	7.44±0.83***	6.96±0.34***	11.14±0.70
GLB	19.93±3.21	14.22±0.58*	16.74±1.03*	17.59±0.74*	13.10±0.60***	13.02±1.12***	17.90±0.68
γ-GT	24.59±2.76	24.38±1.57	21.90±2.43	25.09±2.78	23.64±0.97	21.80±2.45	26.30±2.50
ALT	2.34±0.85	2.08±0.19*	1.98±0.40*	2.16±0.19	2.18±1.05	1.94±0.50*	3.22±0.60
AST	232.88±8.51	219.92±9.06*	235.62±16.55	253.6±13.51	220.10±9.13*	229.14±8.26	253.84±15.80
ALP	12469.16±1522.04**	13683.60±1363.20***	9717.34±1348.33	7404.94±920.27	14237.9±1234.62***	14192.14±1297.87***	6820.24±1794.24
LDH	2365.36±198.41	2026.98±118.58	2277.9±120.87	2458.44±84.64	1968.60±201.40	2094.68±310.05	2137.66±575.27
Urea	1.00±0.06	0.99±0.08	0.95±0.06	0.92±0.04	0.99±0.09	0.93±0.04	0.96±0.13
UA	308.32±205.27	414.22±21.17	353.98±19.02	283.62±12.59	446.38±105.48	367.96±63.08	281.80±74.81
TC	4.79±0.26**	3.15±0.13**	3.56±0.40	3.96±0.34	3.31±0.65	3.11±0.28**	4.01±0.30
TG	1.24±0.29	1.64±0.15*	1.46±0.12	1.13±0.18	1.62±0.63	1.01±0.17	0.96±0.31
GLU	14.33±1.03	13.18±0.54	14.47±0.64	14.22±0.57	13.13±0.78	13.37±0.40	14.28±0.61

The data are expressed as mean ± SD, n =5; compared with IBV group, significance of differences is marked as

\*  $p < 0.05$   
 \*\*  $p < 0.01$   
 \*\*\*  $p < 0.001$ .

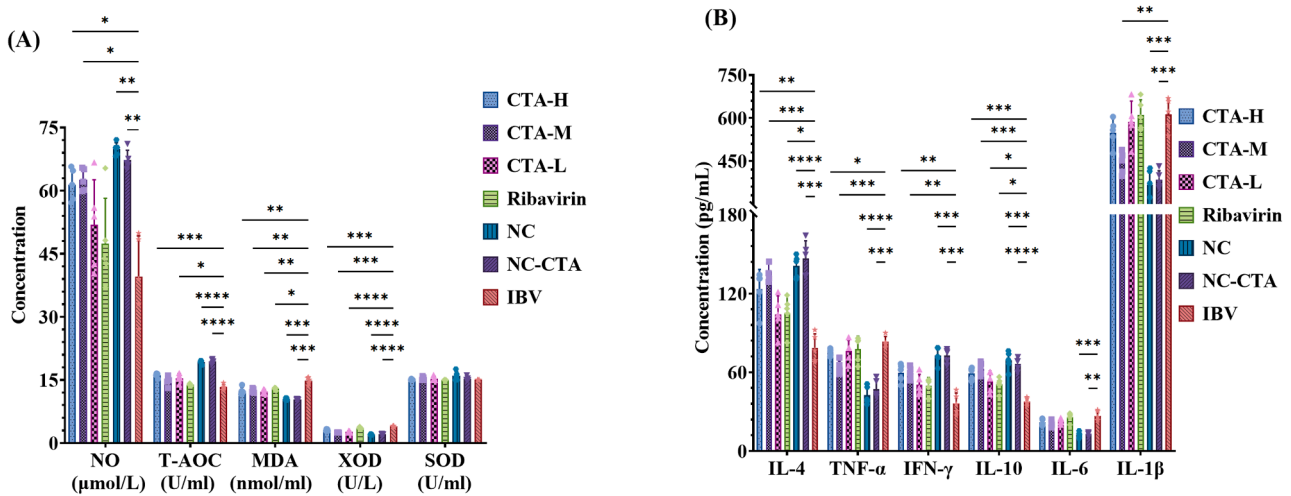


**Fig. 5.** (A) Oxidation factor index; (B) Inflammatory factor markers. Samples with an OD450 value less than 0.3 were considered negative for anti-IBV antibodies. The data are expressed as mean ± SD, n = 5; compared with IBV group, significance of differences is marked as \*  $p < 0.05$ , \*\*  $p < 0.01$ , \*\*\*  $p < 0.001$ .

spectrometer, where data was collected through continuous scanning to obtain the Base peak chromatogram (Fig. 7A-B). A detailed quantitative list of substances can be found in Supplementary Materials 2. The QC model demonstrated stable and reliable performance (taking positive ions as an example, Fig. 7C), and the goodness of fit and prediction ability results indicated that the sample was not overfitted (Fig. 7D). A total of 291 blood components were identified through non-targeted metabolomics (Supplementary Materials 3). The Venn plot of differential metabolites is shown in Fig. 7E, while Fig. 7F presents the number of differential metabolites, with red indicating up-regulation and blue indicating down-regulation. Additionally, Fig. 7G depicts a heat map of bidirectional clustering of samples and differential metabolites. To evaluate the role of the differential metabolite list in biological reactions, KEGG pathway enrichment analysis was performed using MetaboAnalyst (Fig. 7H, Supplementary Materials 4). The experimental results demonstrate that abnormal metabolites interfere with various metabolic pathways, with the Citrate cycle (TCA cycle) being the most significant.

**Network pharmacology analysis.** Network pharmacology analysis was conducted using non-targeted metabolomics data on blood components. Compounds involved in pathways with a significance level of  $P \leq 0.05$  on the KEGG enriched pathways were selected and imported

into SwissTargetPrediction for network pharmacology analysis to obtain relevant data on drug targets (Supplementary Materials 5). The analysis included a total of 40 compounds, and duplicate target proteins were removed, resulting in 528 unique target proteins. These target proteins were used to create a CTA self-built database. To identify target proteins associated with IBV, the GeneCard database and OMIM database were searched using the keyword “infectious bronchitis virus”. Genes obtained from these databases were combined and duplicate genes were eliminated to identify relevant target proteins of IBV (Supplementary Materials 6). A Venn diagram was used to identify key target proteins of CTA and related target proteins of IBV, revealing a total of 159 genes in CTA that are active components in dealing with IBV. Fig. 8A illustrates the construction and intersection of drug-disease targets using Cytoscape to construct a protein-protein interaction (PPI) network.

To further investigate the relationship between terms, enrichment analysis was conducted on 159 intersection targets. The Kappa score, which measures the similarity between words, was calculated using the metascape website. A rich term similarity network was constructed, and the analysis process is detailed in Fig. 8B and Supplementary Materials 7. In this network, each node represents a term and is evaluated based on its cluster ID and  $P$ -value (importance). The size of the nodes indicates the degree of enrichment ( $P$ -value). Larger nodes represent higher

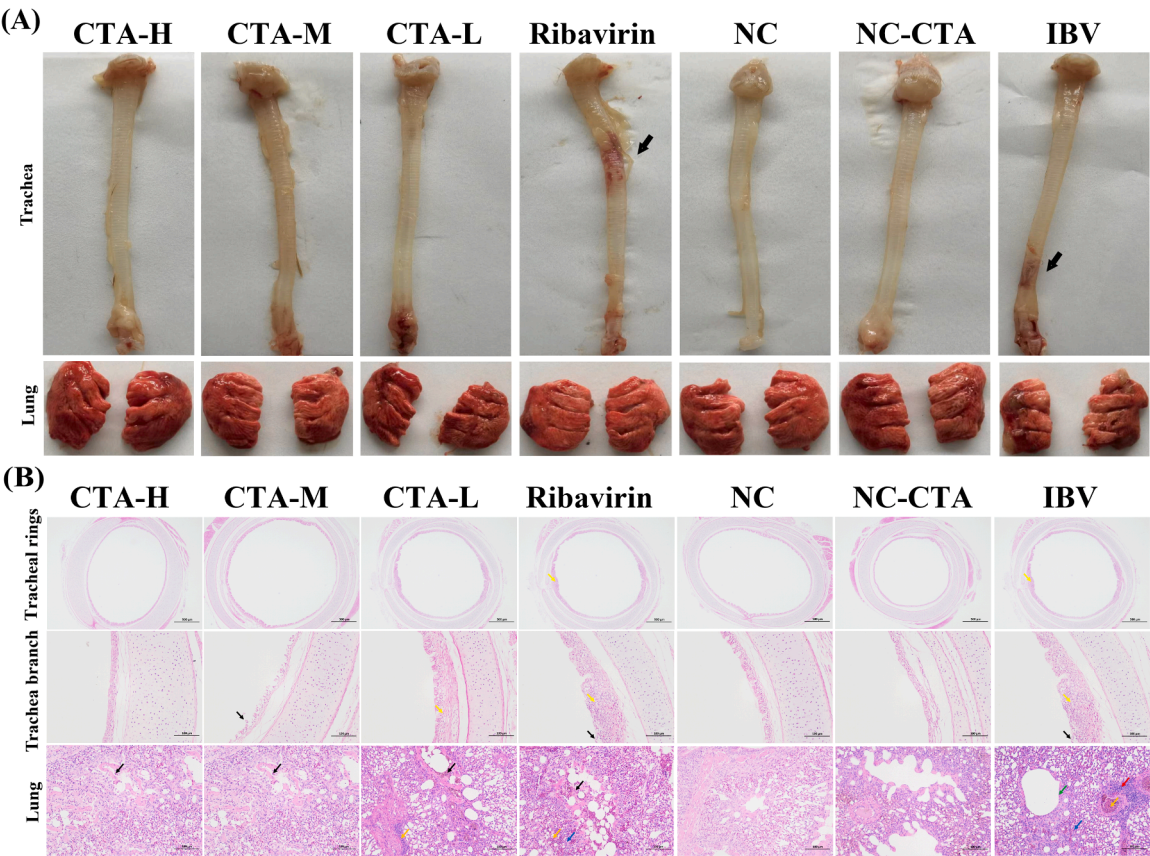


**Fig. 6.** Pathological lesions in the trachea and lungs of IBV-infected chickens. (A) Appearance of the trachea and lungs in each group. Obvious lesions appeared in the IBV group, and the black arrows indicate the presence of mucus and bleeding in the trachea; (B) Pathological sections of tracheal midcircle and lung were examined. In tracheal ring cross-sections and partially magnified sections, black arrows indicated loss of villi or epithelial cells, while yellow arrows indicated lymphocytic infiltration. In the lung section, black arrows pointed out hemorrhage, orange arrows indicated perivascular edema, green arrows highlighted bronchiectasis caused by increased goblet cells, blue arrows showed mild wall thickening, and yellow arrows pointed out necrotic cell debris. Additionally, red arrow indicated lymphocytic infiltration.

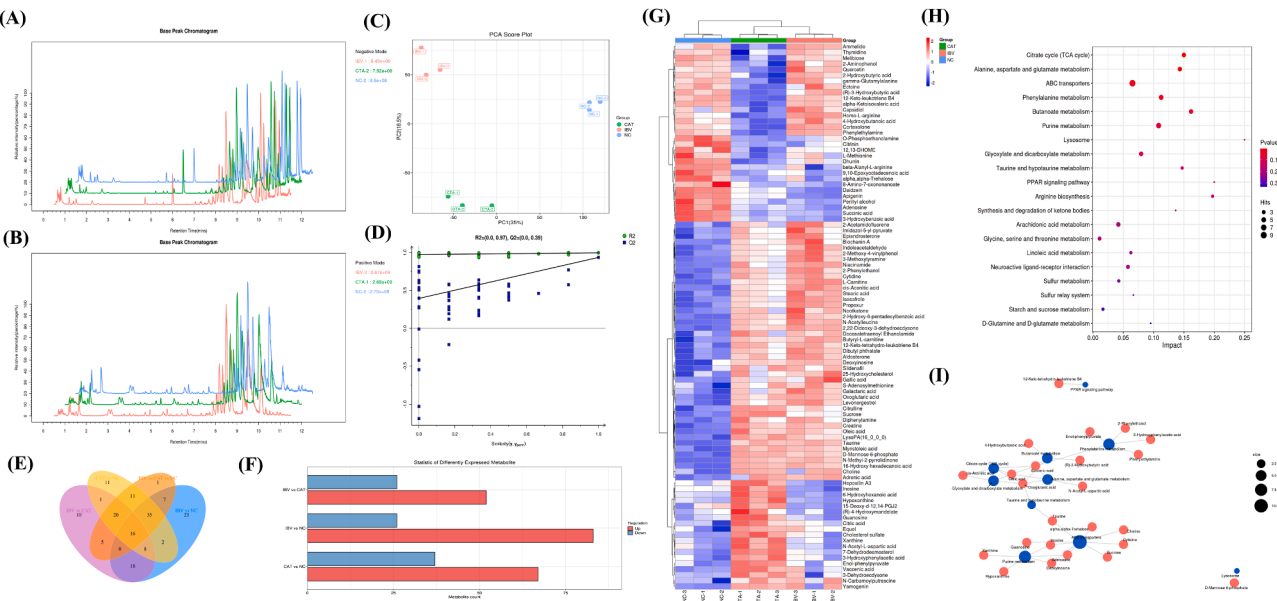


**Fig. 7.** Data analysis of untargeted metabolomics. (A-B) Base peak chromatogram; (C) PCA score plot; (D) PLS-DA permutation test plot; (E) Venn diagram of differential metabolites; (F) Statistical plot of differential metabolite numbers, with the X-axis indicating differential metabolism. The number of compounds, the Y-axis represents the comparison group; (G) Differential metabolite clustering heat map, where the columns represent samples and the rows represent metabolites; (H) Metabolic pathway impact factor bubble chart, the abscissa is the enrichment into different metabolic pathways. The Impact value in The number of metabolites, red indicates differential up-regulation, and blue indicates differential down-regulation.

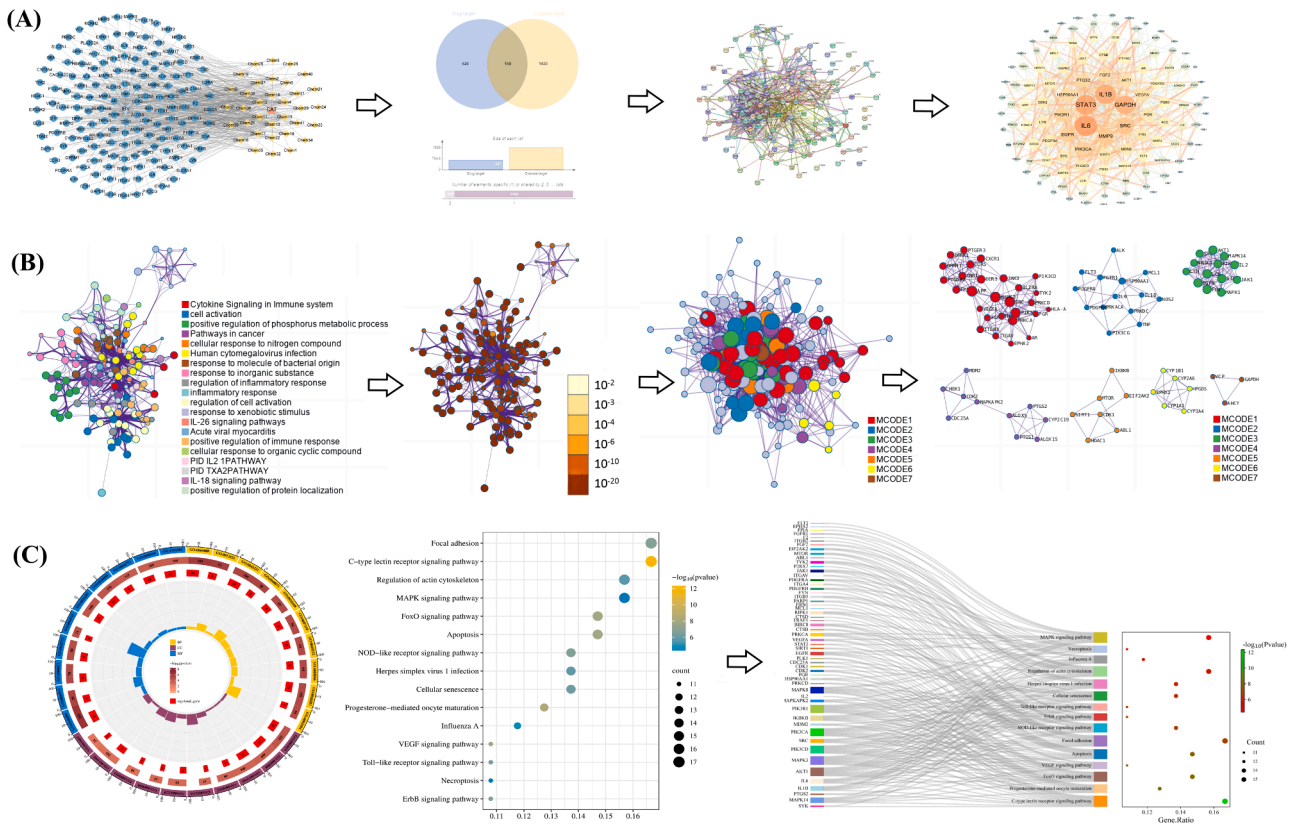


**Fig. 8.** (A) Association between drug targets and disease targets and construction of drug target protein-IBV differential protein interaction (PPI) network. The study constructed a library of drug targets and disease targets, obtained the Wayne intersection, and imported it into the database to obtain the interaction relationships between proteins; (B) GO analysis. (C) Sankey diagram illustrating the correspondence between enrichment-based GO functions and KEGG pathways and involved target proteins. The bubble plot shows the functional description, the color depth represents the P value, and the diameter size represents the number of cross-targets in the current GO function or KEGG pathway.

enrichment of the terms they represent and shorter distances between functionally similar channels. For clarity, only one term label per cluster is shown, and the cluster details are listed in Supplementary Materials 8. The findings revealed that the most enriched clusters were related to cytokine signalling in the immune system. These signals lead to cellular activation through interleukins.

GO terms indicate that these genes are involved in the regulation of biological quality and the metabolic process of purine-containing compounds. They are also associated with cytosol and plasma membranes. The mode of action may involve the catalytic activity of a protein, such as protein tyrosine kinase activity (Fig. 8C, Supplementary Materials 9). The Sankey diagram results from KEGG reveal that the target genes are enriched in multiple pathways. The size of the dots in the KEGG plot represents the number of target genes in each pathway. The main pathway studied is shown on the right side of the Sankey diagram. The study found that CTA is associated with different levels of enrichment in various signaling pathways, including the C-type lectin receptor signaling pathway, Progesterone-mediated oocyte maturation, and FoxO signaling pathway (Fig. 8C, Supplementary Materials 10). On the left side of the Sankey diagram, the target proteins on the corresponding pathway are depicted.

**Joint analysis.** Using a P-value  $\leq 0.05$  as the screening criterion for non-targeted metabolomics analysis, the study identified key metabolic pathways and related metabolites. Specifically, a total of 5 pathways: Citrate cycle (TCA cycle), Alanine aspartate and glutamate metabolism, ABC transporters, Phenylalanine metabolism, and Butanoate metabolism. These pathways involve 20 compounds such as Oxoglutaric acid, Sucrose, and Succinic acid. Additionally, using swisstargetprediction, the study predicted 265 related targets for these compounds. Furthermore, through network pharmacology analysis, we identified the top 10

GO and KEGG results, which revealed that 36 targets are involved in biological processes (BP), 28 targets in cellular components (CC), 34 targets in molecular functions (MF), and 84 targets in KEGG pathways. Notably, among the 20 key non-targeted metabolomics compounds and the 27 compounds involved in network pharmacology, 2 compounds, Inosine and Sucrose, were found to overlap (Supplementary Materials 11).

To investigate the key targets involved in CTA, the study analyzed by intersecting the predicted targets from untargeted metabolomics and network pharmacology. The targets were screened using eight algorithms from the cytohubba plug-in, resulting in the identification of 5 key targets among the top 10 (Fig. 9A). The intersection of these targets revealed points of interest (Fig. 9B). Further GO and KEGG re-enrichment analysis of the five key targets showed their association with the FoxO signaling pathway, Glycolysis/Gluconeogenesis, Biosynthesis of amino acids, and Adipocytokine signaling pathway (Fig. 9C). Molecular docking was then conducted using Discover on two key compounds and five key targets (GAPDH PDB: 1U8F; STAT3 PDB: 5AX3; EGFR PDB: 2GS6; CDK2 PDB: 1AQ1; HSP90AA1 PDB: 1BYQ) to identify the best docking site. The docking binding mode was analyzed and visualized using PyMol, and the docking scores were represented as a heat map. Molecular docking utilizes the docking conformations generated by software for visualization, to examine the binding mode of the ligand in the receptor's active site. Each docking conformation will have a score indicating the binding free energy or other related energy of that conformation. Molecular docking score is a numerical indicator used to evaluate the binding affinity between a ligand and a receptor. The lower the score (usually a negative value), the higher the binding affinity, indicating a more stable interaction between the ligand and the receptor. Fig. 9D-E, Supplementary Materials 12 shows that, all



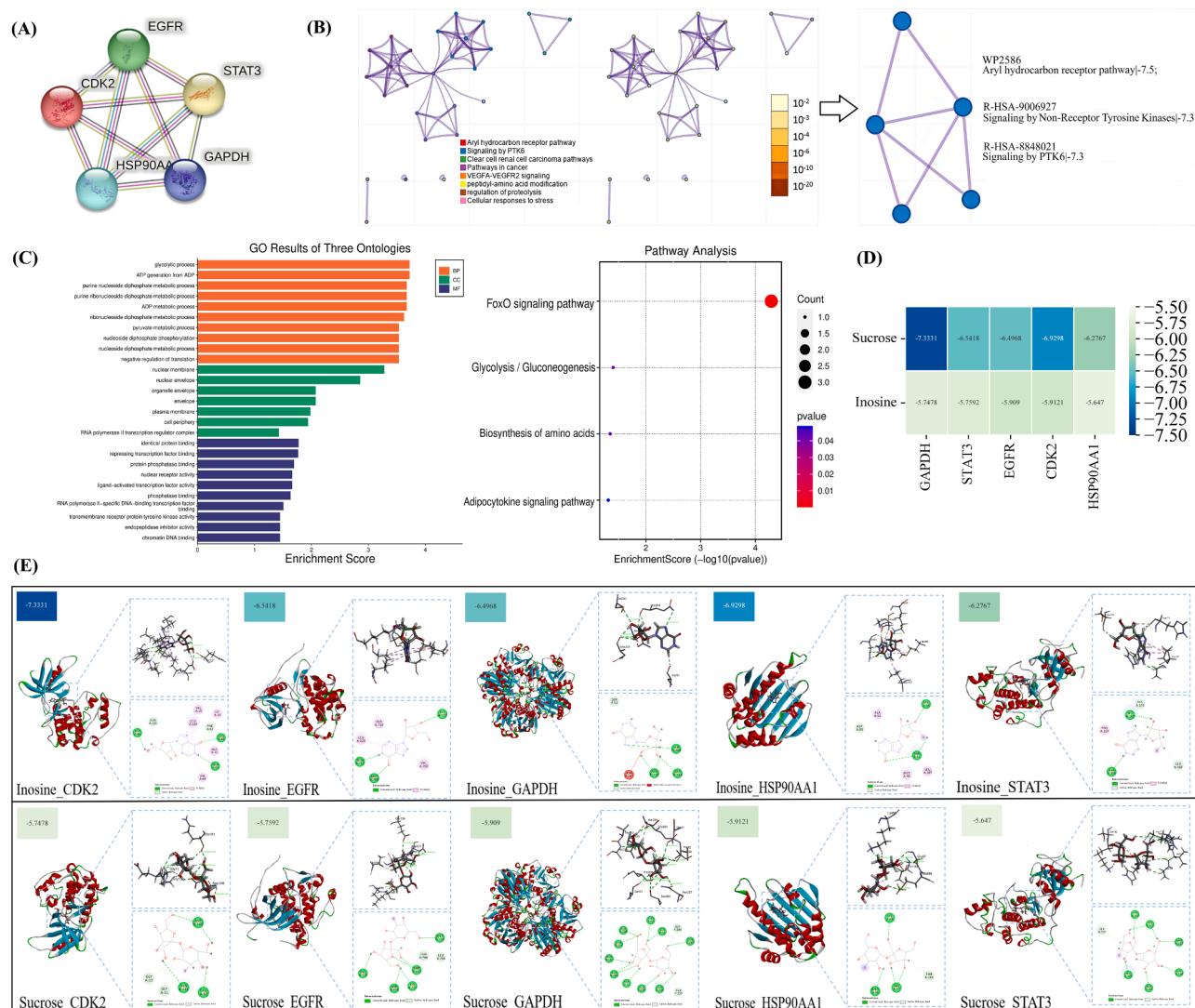


**Fig. 9.** (A) Association diagram of five target proteins that intersect on the main pathways of network pharmacology and metabolomics; (B) Biological Interpretation and PPI Network & MCODE Components are obtained based on the core target, and the circles are colored accordingly to indicate the cluster id. Nodes with the same cluster ID are usually close to each other. In the middle is a network diagram based on enrichment. The darker the color, the more genes are enriched in the pathway. On the right is the best MyList result; (C) Enrichment analysis of five proteins, resulting in GO histogram and KEGG bubble chart; (D) Heatmap of molecular docking scores for key compounds and target proteins; (E) Molecular docking structure display of key compounds and target proteins.

compounds and target proteins demonstrated good docking scores (absolute value  $\geq 5$  as the effective reference range).

Sucrose is an organooxygen compound that affects carbohydrate metabolism and membrane transport, while inosine is a purine nucleoside that affects membrane transport and nucleotide metabolism. These two compounds present a positive correlation in the differential metabolite association heat map and, in complex metabolic network analysis, may mean that they have similar regulatory mechanisms in metabolic pathways or that they are involved in the same biological processes (Fig. 10A). In untargeted metabolomics, the common and only corresponding metabolic pathway between the two is ABC transporters ( $P$ -value=0.02, Supplementary Materials 4). The five key targets show good scores in molecular docking, with a reference value of  $\leq -5$ . Among the pathways involved, the FoxO signaling pathway has the highest overall molecular docking score ( $P$ -value=1.09 $\times 10^{-8}$ ). The target proteins on this pathway are EGFR, STAT3, and CDK2. In summary, after CTA enters the body, it may primarily regulate EGFR, STAT3, and CDK2 proteins through sucrose and inosine, thereby affecting ABC transporters and the FoxO signaling pathway (Fig. 10B).

**Key target verification.** The study focused on the EGFR, STAT3, and

CDK2 proteins in the trachea, which is the target organ of IBV. The study also verified their common downstream product, FOXO. Following the guidance of KEGG, the study selected FOXO3 for verification and further analyzed the phosphorylation of the protein under specific conditions. The results showed an upward trend in the qPCR of the four target genes (Fig. 11A). Through WB verification (Fig. 11B), it was observed that both EGFR and CDK2 proteins exhibited a significant upward trend, while pFOXO decreased in a dose-dependent manner. STAT3 showed a slight increase, and FOXO demonstrated a slightly noticeable upward trend during the process. These findings are consistent with the predictions made by network pharmacology.

## Discussion

IBV presents a significant challenge to the poultry industry, as it causes respiratory diseases that greatly impact the poultry meat industry and global trade (Bande et al., 2017; Zhang et al., 2020). The diversity and frequent genetic mutations of IBV make existing vaccines less effective and complicate prevention and control strategies (Bande et al., 2017; Mork et al., 2014; Valastro et al., 2016). Furthermore, these



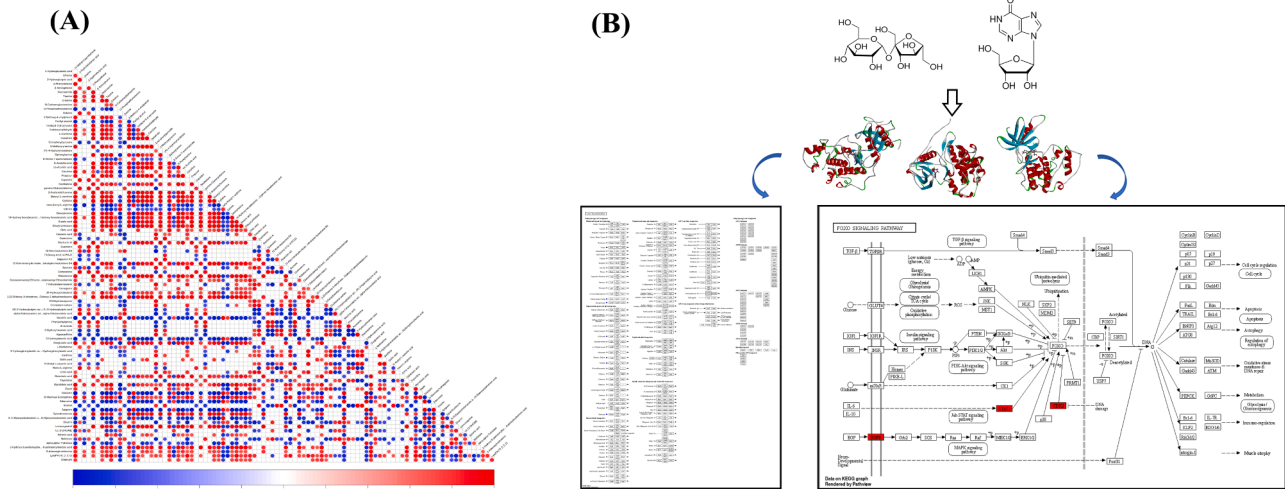


**Fig. 10.** (A) The differential metabolite association heat map of Sucrose and Inosine shows a positive correlation; (B) Non-targeted metabolomics combined with network pharmacology analysis revealed that the key compounds Sucrose and Inosine compounds regulate EGFR, STAT3 and CDK2 Key target proteins affect ABC transporters and FoxO signaling pathways.

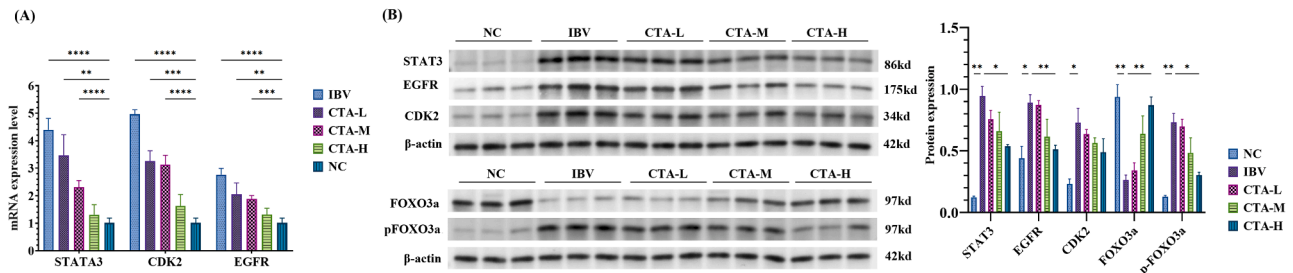


**Fig. 11.** (A) Detection of key target gene expression levels in chick trachea through qPCR experiment, n=5; (B) Detection of the expression levels of key proteins in chick trachea and their co-regulated FOXO protein expression through WB experiment, n=3.

mutations hinder drug development and limit the long-term effectiveness of treatments(Xu et al., 2023). Chinese herbal treatments have shown promise in addressing the IBV challenge(Feng et al., 2021; Yin et al., 2011). Studies have discovered that the active ingredients in Chinese herbal medicine can work in various ways, such as inhibiting viral replication(Yin et al., 2017), reducing inflammation(Chiu et al., 2018), and enhancing immune response(Liu et al., 2023). These findings suggest a new treatment approach: using Chinese herbal medicine instead of traditional antibiotics to reduce the risk of drug resistance and minimize antibiotic usage(van Wietmarschen et al., 2022). However, the incorporation of traditional Chinese medicine into poultry disease management requires extensive research to ensure its efficacy and safety(Domingues et al., 2022). It should also be integrated with existing prevention and control measures to promote the sustainable and healthy development of the poultry industry.

The integration and analysis of rich traditional Chinese medicine knowledge base and data in the traditional Chinese medicine inheritance computing platform is of significant importance to the research and development of new drugs(Dai et al., 2018). This platform can assist researchers in exploring potential drug resources. As a result, it accelerates the discovery process of new drugs, reduces research and development costs, and promotes the modernization and internationalization of traditional Chinese medicine. This study utilizes big data from the TCMICS V3.0 to screen TCM prescriptions with similar symptoms among the marketed drugs for constructing a model of IBV based on clinical characteristics. A traditional Chinese medicine prescription, CTA, was generated and verified, consisting of rehmannia glutinosa, fritillaria fritillary, ophiopogon japonicus, licorice, borneol, and bitter almond as ingredients. Each ingredient has different effects. Rehmannia glutinosa

has heat-clearing, detoxifying, anti-inflammatory, and immunity-enhancing effects, which can reduce inflammatory symptoms and resist bronchitis infections(Janssen et al., 2020). Fritillaria fritillary has the effects of clearing away heat and resolving phlegm, moistening the lungs, and relieving coughs. It can inhibit the inflammatory reaction, promote the discharge of phlegm, and reduce the symptoms of cough and excessive phlegm(Pai et al., 2023). Ophiopogon japonicus has the effects of nourishing yin, moistening dryness, producing body fluids, and quenching thirst, and can relieve dry mouth, sore throat, and heat sensation(Chen et al., 2016). Licorice has anti-inflammatory, analgesic, and immunomodulatory effects that can reduce inflammatory symptoms and enhance immunity(Yang et al., 2015). Borneol has the effects of clearing heat, detoxifying, analgesic, relieving cough, and asthma, and can relieve symptoms such as fever, cough, and asthma(Mei et al., 2023). Bitter almonds have antitussive and expectorant properties, which can reduce cough and phlegm production and relieve bronchitis symptoms(Wei et al., 2023). Upon identification of traditional Chinese medicine ingredients, it was discovered that this compound contains 484 active compounds. These include 67 types of Carboxylic acids and derivatives, 45 types of Benzene and substituted derivatives, and 43 types of Fatty Acyls. These ingredients have proven to be beneficial in the treatment of bronchitis(Fouladi et al., 2019; Zhang et al., 2023). They exert therapeutic effects by inhibiting inflammatory reactions, clearing heat and detoxifying, moisturizing the lungs, relieving coughs, and enhancing immunity.

*In vitro* experiments provide researchers with precise control over the experimental environment, enabling them to study the effects of specific variables on cells or molecules. To verify the therapeutic effect of CTA *in vitro*, three commonly used models for studying IBV were selected for

analysis: CEK cells(Chen et al., 2019a), tracheal rings(Pei et al., 2001), and chicken embryos(Reynolds and Simpson, 2022). The maximum safe dose of CTA on cells was determined to be 25 mg/mL, and its antiviral effect on CEK cells was comparable to that of ribavirin. In the tracheal ring experiment, CTA exhibited a better protective effect on tracheal villi compared to ribavirin, thereby preventing damage to the trachea by IBV to a certain extent. Furthermore, in chicken embryos, CTA demonstrated a stronger protective effect than ribavirin and improved the survival rate of the embryos. The EI index provided evidence that CTA can enhance the condition of stiff seedlings.

*In vivo* experiments have demonstrated that CTA exhibits antiviral potential at specific doses. Particularly, CTA-H has a significant therapeutic effect on IBV, effectively relieving symptoms and improving production performance. Immune organ indexes, such as the size and weight of the spleen, thymus, and bursa of Fabricius, serve as important indicators for evaluating the immune status of animals and reflect the strength of immune function. CTA can significantly promote the development of immune organs and enhance cellular and humoral immune functions. This may be attributed to the decomposition of active ingredients of CTA in the intestines, providing necessary nutrients for the growth of immune organs. To verify the inhibitory effect of CTA *in vivo*, the study employed RT-qPCR to measure viral mRNA levels in the trachea and lungs of different groups of chicks. The results demonstrated that CTA caused a decrease in viral mRNA levels, particularly at 3dpi, when compared to the challenge control group. Moreover, the treatment effects of different drug groups on the trachea of chicks were similar at 7dpi and 14dpi. In the defense against IBV infection, high antibody levels play a crucial role in humoral immunity and form the core of the defense mechanism(Chhabra et al., 2015). Studies have indicated that traditional Chinese medicine can enhance cellular and humoral immune responses in chickens(Lee et al., 2011). This study found that CTA treatment significantly increased the IBV antibody titer in the serum when compared to the untreated control group, with its level being notably higher than that of the prevention group and positive control group. These findings further support the potential of traditional Chinese medicine to improve humoral immunity.

Excessive oxidative stress induced by chicken coronavirus can result in the overproduction of reactive oxygen species in chickens(Feng et al., 2022). These reactive oxygen species have the potential to harm cell structures, including lipid membranes, proteins, and DNA, leading to cell death and tissue damage(Greenberger et al., 2001). As a result, the growth, development, immune function, and production performance of chickens can be affected. In severe cases, excessive immune system activation and a subsequent systemic inflammatory response can worsen the disease. MDA, a byproduct of lipid peroxidation, is often considered an indicator of cell membrane damage and increased oxidative stress(Niedernhofer et al., 2003). Elevated XOD activity can contribute to the generation of uric acid and reactive oxygen species, further exacerbating oxidative damage(Kim et al., 2001). In this study, CTA was found to significantly reduce the expression levels of MDA and XOD in diseased chickens. T-AOC represents the overall defense level of antioxidants in the body, and CTA was found to increase its expression(El-Senousey et al., 2018). Moreover, CTA-H and CTA-M were observed to further enhance the expression level of NO. Excessive inflammation can lead to an increase in cytokines, impair immunity, and cause significant harm to the host(Chaudhary et al., 2023; Kaur et al., 2020). Research indicates that coronaviruses can evade host defenses by elevating pro-inflammatory factors and reducing the production of type 1 interferons(Kint et al., 2016; Mahallawi et al., 2018). In the context of IBV infection, the application of CTA was found to significantly elevate the levels of anti-inflammatory factors such as IL-4, IFN- $\gamma$ , and IL-10, while reducing the expression of pro-inflammatory factors like TNF- $\alpha$ , IL-6, and IL-1 $\beta$ , thereby improving the cell-mediated immune response. Maintaining a balance between pro- and anti-inflammatory factors is crucial in combating coronavirus infections. Pathological sections demonstrate that CTA can mitigate the damage to the trachea and lungs

caused by IBV.

Traditional Chinese medicine may be safe for humans, but it can cause discomfort in chickens, especially drug-sensitive chicks. In China, some veterinarians have developed a unique therapeutic system for animal diseases by integrating the physiological characteristics of animals with TCM treatment principles. Although no direct applications of TCMICS V3.0 in veterinary medicine have been found in the literature, the software holds significant potential to advance veterinary drug development. TCMICS V3.0 is regarded as an important tool for preserving TCM academic thought and clinical experience, and has been used in the inheritance of TCM knowledge, the analysis of TCM literature, and the development of TCM products(Tang and Yang, 2024). Similarly, by using this software to analyze the efficacy of traditional Chinese medicines for treating animal diseases, it could facilitate the discovery of new veterinary treatments. Additionally, the system could enhance drug formulations by identifying synergistic combinations of herbal ingredients, thus improving therapeutic outcomes, reducing side effects, and potentially preventing adverse drug reactions in animals caused by certain TCM components. TCMICS offers solutions for bronchitis in chickens using data from the Veterinary Pharmacopoeia and traditional Chinese medicine compounds, emphasizing the importance of strictly reviewing the safety of chicks. Monitoring blood routine and biochemistry test data during treatment is essential to assess the impact, track effectiveness, and make necessary adjustments to ensure both efficacy and safety(Lin et al., 2020). The study compared the CTA treatment group with the IBV infection group, revealing significant differences in most serum biochemical indicators, except for  $\gamma$ -GT, LDH, Urea, UA, and GLU. Concurrent changes in hematological parameters such as RBC, PLT, HTC, PCT, and GRAN% indicate that CTA-M may help mitigate blood system alterations caused by IBV infection. These significant indicators suggest that CTA-M treatment could potentially help maintain blood homeostasis, enhance immune response, and partially shield chickens from severe physiological damage induced by IBV.

Network pharmacology combined with non-targeted metabolomic analysis offers a systematic approach to uncover the comprehensive mechanism of action of drugs, aiding in the evaluation of both target effects and metabolic effects(Qiu et al., 2023). This method not only elucidates the drug-target protein interactions and metabolic pathway regulations but also enhances individualized treatment for chickens infected with infectious bronchitis virus(Noor et al., 2023). By analyzing individual metabolic variations and predicting drug effects, this strategy facilitates the optimization of treatment plans. Previous research has highlighted various antiviral mechanisms of plant extracts against avian infectious bronchitis virus, including interference with viral replication(Wani et al., 2021), structural damage to the virus(Chen et al., 2014), dissolution of the IBV envelope(Lelesius et al., 2019), and direct virucidal effects(Yin et al., 2011). To investigate the mechanism of action of CTA against IBV, this study unveiled the potential biological mechanism of CTA through a combined analysis of non-targeted metabolomics and network pharmacology. Using a screening criterion of  $P$ -value  $\leq 0.05$ , the study identified 5 key metabolic pathways and 20 related metabolites. Through eight algorithm screenings with the CytoHubba plug-in, the study pinpointed 5 key targets, namely GAPDH, STAT3, EGFR, CDK2, and HSP90AA1. Docking scores and Pymol visualization results demonstrated that the key compounds in CTA can effectively interact with these target proteins. The joint analysis indicated that the compounds sucrose and inosine may play crucial roles in the ABC transporter and FoxO signaling pathways, with EGFR, STAT3, and CDK2 identified as key targets.

ABC transporters play a crucial role in drug antiviral research by influencing drug absorption, distribution, metabolism, and excretion in the body(Szakacs et al., 2008). These proteins impact drug transport within and between cells, consequently affecting drug efficacy and metabolism. Studies indicate that ABC transporters can reduce drug effectiveness by removing drugs from cells and lowering their concentration in the body(Gil-Martins et al., 2020; Schinkel and Jonker, 2003).

Understanding the significance of ABC transporters in drug research is essential for developing more potent antiviral medications. Non-targeted metabolomics KEGG results suggest that CTA could potentially enhance drug concentration and residence time in the body by inhibiting the ABC transporter pathway. This inhibition may improve drug absorption, bioavailability, and therapeutic effects against viruses (Higgins, 2001). These findings offer valuable insights for discovering new antiviral drugs or enhancing the efficacy of existing ones.

FoxO is a crucial transcription factor involved in various biological processes including cell cycle, proliferation, apoptosis, and oxidative stress resistance (Kaestner et al., 2000). STAT3 is a key signal transduction protein that plays a significant role in receiving and relaying extracellular signals (Yamauchi-Takahara and Kishimoto, 2000). When STAT3 is downregulated, it can enhance the transcriptional regulatory function of the FoxO protein and facilitate its nuclear localization (Guo et al., 2018). EGFR, a proto-oncogene, induces cell proliferation and migration by binding to ligands (Wang et al., 2018). Activation of EGFR triggers STAT3 phosphorylation, influencing its localization and function (Bhat et al., 2018). CDK2 is a pivotal member of cell cycle-dependent protein kinases (CDKs) and is essential for cell cycle progression (Enders, 2012; Malumbres and Barbacid, 2009). In the FoxO pathway, the downregulation of EGFR and CDK2 results in FoxO protein dephosphorylation, promoting its nuclear translocation and enhancing its transcriptional regulatory capacity (Huang et al., 2006; Saxena et al., 2013). This can lead to interactions with other transcription factors, coactivators, or nuclear receptors, impacting their regulatory network and key biological processes such as cell proliferation, metabolism, and stress response (Su et al., 2024). Experimental evidence using qPCR and WB techniques demonstrated that CTA can downregulate EGFR, STAT3, and CDK2 expression by modulating sucrose and inosine levels, leading to FoxO dephosphorylation and nuclear translocation. This regulatory mechanism influences cell cycle, apoptosis, antioxidant stress, and cell differentiation, enhancing resistance to oxidative stress and upregulating anti-inflammatory factors to inhibit viral growth and proliferation.

This study introduced a novel antiviral compound called CTA, derived from an IBV prescription dataset. Although this study primarily focuses on the efficacy of CTA against avian infectious bronchitis virus, we acknowledge the importance of its toxicity and safety. The complexity and multi-component nature of the traditional Chinese medicine formulation mean that its pharmacological and toxicological effects may be multifaceted, particularly in cases of different dosages, varying treatment durations, or co-administration with other drugs, which may lead to adverse or toxic reactions. In this study, CTA demonstrated significant antiviral properties both *in vitro* and *in vivo*, confirming its safety for chicks at the administered doses. However, future systematic toxicity studies are necessary, including investigations into acute toxicity, subchronic toxicity, chronic toxicity, as well as teratogenicity and carcinogenicity, in order to comprehensively assess the safety of CTA and provide a scientific basis for its clinical promotion and large-scale application. The compound appears to influence the EGFR, STAT3, and CDK2 proteins through the regulation of sucrose and inosine, subsequently impacting the ABC transporter metabolic pathway and FoxO signaling pathway. These findings lay a solid foundation for further investigating the pharmacodynamic mechanisms of CTA.

Given the complexity of natural plant aqueous extracts, the structure-activity relationship (SAR) of CTA compounds derived from various plant sources is essential in the drug design and development process. This study specifically reflects its application in the genetic analysis of traditional Chinese medicine. The platform integrates data from untargeted metabolomics and network pharmacology to conduct relevant pathway analyses and predict the compounds involved. This research represents the first analysis utilizing a traditional Chinese medicine genetic computing platform to examine natural plant-derived mixtures administered to animals. While subsequent studies have primarily verified the FoxO pathway, it is important to acknowledge that the protective effect mediated by CTA is also associated with metabolic

processes. However, the precise influence of fluctuations in these metabolites on viral replication remains unclear, as does their potential role in viral replication or immune regulation. Future research should delve deeper into the specific functions of these pathways and targets in the therapeutic effects of CTA, as well as investigate their potential interactions. These findings were employed to optimize the composition and extraction process of CTA, paving the way for further detailed pharmacokinetic and pharmacodynamic studies on the enhanced CTA.

## Conclusion

In summary, this study introduced a new antiviral compound, CTA, derived from an IBV prescription dataset. CTA demonstrated significant antiviral properties both *in vitro* and *in vivo* while remaining safe for chicks at the dosages administered. The mechanism of action of CTA involves the regulation of sucrose and inosine, leading to an impact on EGFR, STAT3, and CDK2 proteins. This subsequently affects the ABC transporter metabolic pathway and FoxO signaling pathway. These findings lay a solid foundation for further investigation into the pharmacodynamic mechanism of CTA and its clinical application in IBV prevention and treatment.

## Web links and URLs

Chinese medicine prescription database (<https://db.yaozh.com>)  
 The preparation data (<http://cpmtp.wangk.pro>)  
 HMDB (<http://www.hmdb.ca>) massbank (<http://www.massbank.jp/>)  
 LipidMaps (<http://www.lipidmaps.org>) mzccloud (<https://www.mzcloud.org>)  
 KEGG (<https://www.genome.jp/kegg/>)  
 Swiss Target Prediction Server (<http://www.swisstargetprediction.ch/>)  
 Gene Cards (<https://www.genecards.org/>)  
 OMIM (<https://omim.org/>)  
 Venny 2.1 software (<https://bioinfo.gp.cnb.cic.es/tools/venny/>)  
 String database (<https://www.string-db.org/>) metascap website (<http://metascap.org>)

## Declaration of competing interest

We declare that we have no financial and personal relationships with other people or organizations that can inappropriately influence our work, and there is no professional or other personal interest in any nature or kind in any product, service and/or company that could be construed as influencing the content of this paper.

## Acknowledgements

Funding is supported by the earmarked fund for CARS-Guangxi Poultry Industry Innovation Team (nycytgxxt-2024-19-2), National Nature Foundation United Fund U22A20523), Central Government-guided Local Science and Technology Development Fund (Guike ZY23055041), Guangxi University Innovation Multiplication Plan (2024BZPT020).

## Supplementary materials

Supplementary material associated with this article can be found, in the online version, at [doi:10.1016/j.psj.2025.104956](https://doi.org/10.1016/j.psj.2025.104956).

## Appendix supplementary data

The datasets supporting the conclusions of this article are included within the article (and its Supplementary Materials).



## References

- Abdelrazig, S., Safo, L., Rance, G.A., Fay, M.W., Theodosiou, E., Topham, P.D., Kim, D.H., Fernandez-Castane, A., 2020. Metabolic characterisation of magnetospirillum gryphiswaldense MSR-1 using LC-MS-based metabolite profiling. *RSC Adv.* 10, 32548–32560. <https://doi.org/10.1039/d0ra05326k>.
- Bande, F., Arshad, S.S., Omar, A.R., Hair-Bejo, M., Mahmuda, A., Nair, V., 2017. Global distributions and strain diversity of avian infectious bronchitis virus: a review. *Anim. Health Res. Rev.* 18, 70–83. <https://doi.org/10.1017/S1466252317000044>.
- Bhat, A.A., Lu, H., Soutto, M., Capobianco, A., Rai, P., Zaika, A., El-Rifai, W., 2018. Exposure of Barrett's and esophageal adenocarcinoma cells to bile acids activates EGFR-STAT3 signaling axis via induction of APE1. *Oncogene* 37, 6011–6024. <https://doi.org/10.1038/s41388-018-0388-8>.
- Bijlenga, G., Cook, J.K., Gelb Jr., J., de Wit, J.J., 2004. Development and use of the H strain of avian infectious bronchitis virus from the Netherlands as a vaccine: a review. *Avian Pathol.* 33, 550–557. <https://doi.org/10.1080/03079450400013154>.
- Chaudhary, R., Meher, A., Krishnamoorthy, P., Kumar, H., 2023. Interplay of host and viral factors in inflammatory pathway mediated cytokine storm during RNA virus infection. *Curr. Res. Immunol.* 4, 100062. <https://doi.org/10.1016/j.crimmu.2023.100062>.
- Chen, C., Zuckerman, D.M., Brantley, S., Sharpe, M., Childress, K., Hoiczky, E., Pendleton, A.R., 2014. Sambucus nigra extracts inhibit infectious bronchitis virus at an early point during replication. *BMC Vet. Res.* 10, 24. <https://doi.org/10.1186/1746-6148-10-24>.
- Chen, H., Feng, R., Muhammad, I., Abbas, G., Zhang, Y., Ren, Y., Huang, X., Zhang, R., Diao, L., Wang, X., Li, G., 2019a. Protective effects of hypericin against infectious bronchitis virus induced apoptosis and reactive oxygen species in chicken embryo kidney cells. *Poult. Sci.* 98, 6367–6377. <https://doi.org/10.3382/pes/pez465>.
- Chen, H., Muhammad, I., Zhang, Y., Ren, Y., Zhang, R., Huang, X., Diao, L., Liu, H., Li, X., Sun, X., Abbas, G., Li, G., 2019b. Antiviral activity against infectious bronchitis virus and bioactive components of Hypericum perforatum L. *Front. Pharmacol.* 10, 1272. <https://doi.org/10.3389/fphar.2019.01272>.
- Chen, M.H., Chen, X.J., Wang, M., Lin, L.G., Wang, Y.T., 2016. Ophiopogon japonicus—A phytochemical, ethnomedicinal and pharmacological review. *J. Ethnopharmacol.* 181, 193–213. <https://doi.org/10.1016/j.jep.2016.01.037>.
- Chen, Y.N., Kao, W.M., Lee, S.C., Wu, J.M., Ho, Y.S., Hsieh, M.K., 2022. Antiviral properties of pennisetum purpureum extract against coronaviruses and enteroviruses. *Pathogens* 11. <https://doi.org/10.3390/pathogens11111371>.
- Cheung, C.L., Rayner, J.M., Smith, G.J., Wang, P., Naipospos, T.S., Zhang, J., Yuen, K.Y., Webster, R.G., Peiris, J.S., Guan, Y., Chen, H., 2006. Distribution of amantadine-resistant H5N1 avian influenza variants in Asia. *J. Infect. Dis.* 193, 1626–1629. <https://doi.org/10.1086/504723>.
- Chhabra, R., Chantrey, J., Ganapathy, K., 2015. Immune responses to virulent and vaccine strains of infectious bronchitis viruses in chickens. *Viral Immunol.* 28, 478–488. <https://doi.org/10.1089/vim.2015.0027>.
- Chiu, Y.J., Lee, C.M., Lin, T.H., Lin, H.Y., Lee, S.Y., Mesri, M., Chang, K.H., Lin, J.Y., Lee-Chen, G.J., Chen, C.M., 2018. Chinese herbal medicine glycyrrhiza inflata Reduces abeta aggregation and exerts neuroprotection through anti-oxidation and anti-inflammation. *Am. J. Chin. Med.* 1–25. <https://doi.org/10.1142/S0192415x18500799>.
- Dai, Q.L., Jiang, F., Wang, J., Gong, C.L., Shi, M.Y., 2018. Based on traditional Chinese medicine inheritance support system to analyze the regularity of umbilicus application to treat ascites due to cirrhosis. *Zhongguo Zhong Yao Za Zhi* 43, 4541–4546. <https://doi.org/10.19540/j.cnki.cjcm.20180912.001>.
- de Wit, J.J., Nieuwenhuisen-van Wilgen, J., Hoogkamer, A., van de Sande, H., Zuidam, G.J., Fabri, T.H., 2011. Induction of cystic oviducts and protection against early challenge with infectious bronchitis virus serotype D388 (genotype QX) by maternally derived antibodies and by early vaccination. *Avian Pathol.* 40, 463–471. <https://doi.org/10.1080/03079457.2011.599060>.
- Dhama, K., Singh, S.D., Barathidasan, R., Desingu, P.A., Chakraborty, S., Tiwari, R., Kumar, M.A., 2014. Emergence of avian infectious bronchitis virus and its variants need better diagnosis, prevention and control strategies: a global perspective. *Pak. J. Biol. Sci.* 17, 751–767. <https://doi.org/10.3923/pjbs.2014.751.767>.
- Dhinakar Raj, G., Kumar, K.Suresh, Nainar, A.M., Nachimuthu, K., 2004. Egg:embryo weight ratio as an indicator of dwarfism induced by infectious bronchitis virus. *Avian Pathol.* 33, 307–309. <https://doi.org/10.1080/0307945042000205883>.
- Domingues, K., Franco, N.H., Rodrigues, I., Stilwell, G., Magalhaes-Sant'Ana, M., 2022. Bibliometric trend analysis of non-conventional (alternative) therapies in veterinary research. *Vet. Q.* 42, 192–198. <https://doi.org/10.1080/01652176.2022.2142318>.
- El-Senousey, H.K., Chen, B., Wang, J.Y., Atta, A.M., Mohamed, F.R., Nie, Q.H., 2018. Effects of dietary vitamin C, vitamin E, and alpha-lipoic acid supplementation on the antioxidant defense system and immune-related gene expression in broilers exposed to oxidative stress by dexamethasone. *Poult. Sci.* 97, 30–38. <https://doi.org/10.3382/ps/pex298>.
- Enders, G.H., 2012. Mammalian interphase cdk: dispensable master regulators of the cell cycle. *Genes Cancer* 3, 614–618. <https://doi.org/10.1177/1947601913479799>.
- Fan, W.S., Li, H.M., He, Y.N., Tang, N., Zhang, L.H., Wang, H.Y., Zhong, L., Chen, J.C., Wei, T.C., Huang, T., Mo, M.L., Wei, P., 2018. Immune protection conferred by three commonly used commercial live attenuated vaccines against the prevalent local strains of avian infectious bronchitis virus in southern China. *J. Vet. Med. Sci.* 80, 1438–1444. <https://doi.org/10.1292/jvms.18-0249>.
- Feng, H., Wang, X., Zhang, J., Zhang, K., Zou, W., Zhang, K., Wang, L., Guo, Z., Qiu, Z., Wang, G., Xin, R., Li, J., 2021. Combined effect of Shengdailong granule and doxycycline on immune responses and protection against avian infectious bronchitis virus in broilers. *Front. Vet. Sci.* 8, 756629. <https://doi.org/10.3389/fvets.2021.756629>.
- Feng, H., Zhang, J., Zhang, K., Wang, X., Zhang, K., Guo, Z., Han, S., Wang, L., Qiu, Z., Wang, G., Li, J., 2022. Phillygenin activates PKR/eIF2alpha pathway and induces stress granule to exert anti-avian infectious bronchitis virus. *Int. Immunopharmacol.* 108, 108764. <https://doi.org/10.1016/j.intimp.2022.108764>.
- Fouladi, S., Masjedi, M., Ganjalikhan Hakemi, M., Eskandari, N., 2019. The review of in vitro and in vivo studies over the glycyrrhizic acid as natural remedy option for treatment of allergic asthma. *Iran. J. Allergy Asthma Immunol.* 18, 1–11.
- Gil-Martins, E., Barbosa, D.J., Silva, V., Remiao, F., Silva, R., 2020. Dysfunction of ABC transporters at the blood-brain barrier: role in neurological disorders. *Pharmacol. Ther.* 213, 107554. <https://doi.org/10.1016/j.pharmthera.2020.107554>.
- Greenberger, J.S., Kagan, V.E., Pearce, L., Boriseniao, G., Tyurina, Y., Epperly, M.W., 2001. Modulation of redox signal transduction pathways in the treatment of cancer. *Antioxid. Redox Signal.* 3, 347–359. <https://doi.org/10.1089/15230860152409004>.
- Guo, F., Yu, X., Xu, A., Xu, J., Wang, Q., Guo, Y., Wu, X., Tang, Y., Ding, Z., Zhang, Y., Gong, T., Pan, Z., Li, S., Kong, L., 2018. Japanese encephalitis virus induces apoptosis by inhibiting Foxo signaling pathway. *Vet. Microbiol.* 220, 73–82. <https://doi.org/10.1016/j.vetmic.2018.05.008>.
- Higgins, C.F., 2001. ABC transporters: physiology, structure and mechanism—an overview. *Res. Microbiol.* 152, 205–210. [https://doi.org/10.1016/s0923-2508\(01\)01193-7](https://doi.org/10.1016/s0923-2508(01)01193-7).
- Horai, H., Arita, M., Kanaya, S., Nihei, Y., Ikeda, T., Suwa, K., Ojima, Y., Tanaka, K., Tanaka, S., Aoshima, K., Oda, Y., Kakazu, Y., Kusano, M., Tohge, T., Matsuda, F., Sawada, Y., Hirai, M.Y., Nakanishi, H., Ikeda, K., Akimoto, N., Maoka, T., Takahashi, H., Ara, T., Sakurai, N., Suzuki, H., Shibata, D., Neumann, S., Iida, T., Tanaka, K., Funatsu, K., Matsuura, F., Soga, T., Taguchi, R., Saito, K., Nishioka, T., 2010. MassBank: a public repository for sharing mass spectral data for life sciences. *J. Mass Spectrom.* 45, 703–714. <https://doi.org/10.1002/jms.1777>.
- Huang, H., Regan, K.M., Lou, Z., Chen, J., Tindall, D.J., 2006. CDK2-dependent phosphorylation of FOXO1 as an apoptotic response to DNA damage. *Science* 314, 294–297. <https://doi.org/10.1126/science.1130512> (1979).
- Jackwood, M.W., 2012. Review of infectious bronchitis virus around the world. *Avian Dis.* 56, 634–641. <https://doi.org/10.1637/10227-043012-Review.1>.
- Janssen, E.M., Dy, S.M., Meara, A.S., Kneuert, P.J., Presley, C.J., Bridges, J.F.P., 2020. Analysis of patient preferences in lung cancer - estimating acceptable tradeoffs between treatment benefit and side effects. *Patient Prefer. Adherence* 14, 927–937. <https://doi.org/10.2147/PPA.S235430>.
- Jordan, B., 2017. Vaccination against infectious bronchitis virus: a continuous challenge. *Vet. Microbiol.* 206, 137–143. <https://doi.org/10.1016/j.vetmic.2017.01.002>.
- Kaestner, K.H., Knochel, W., Martinez, D.E., 2000. Unified nomenclature for the winged helix/forkhead transcription factors. *Genes Dev.* 14, 142–146.
- Kaur, S., Bansal, Y., Kumar, R., Bansal, G., 2020. A panoramic review of IL-6: structure, pathophysiological roles and inhibitors. *Bioorg. Med. Chem.* 28, 115327. <https://doi.org/10.1016/j.bmc.2020.115327>.
- Kim, Y.S., Nam, H.J., Chung, H.Y., Kim, N.D., Ryu, J.H., Lee, W.J., Arking, R., Yoo, M.A., 2001. Role of xanthine dehydrogenase and aging on the innate immune response of drosophila. *J. Am. Aging Assoc.* 24, 187–193. <https://doi.org/10.1007/s11357-001-0020-6>.
- Kint, J., Langereis, M.A., Maier, H.J., Britton, P., van Kuppeveld, F.J., Koumans, J., Wiegertjes, G.F., Forlenza, M., 2016. Infectious bronchitis coronavirus limits interferon production by inducing a host shutoff that requires accessory protein 5b. *J. Virol.* 90, 7519–7528. <https://doi.org/10.1128/JVI.00627-16>.
- Lee, S.H., Lillehoj, H.S., Jang, S.I., Lee, K.W., Bravo, D., Lillehoj, E.P., 2011. Effects of dietary supplementation with phytonutrients on vaccine-stimulated immunity against infection with Eimeria tenella. *Vet. Parasitol.* 181, 97–105. <https://doi.org/10.1016/j.vetpar.2011.05.003>.
- Lelesius, R., Karpovaite, A., Mickiene, R., Drevinskas, T., Tiso, N., Ragazinskiene, O., Kubiliene, L., Maruska, A., Salomskas, A., 2019. In vitro antiviral activity of fifteen plant extracts against avian infectious bronchitis virus. *BMC Vet. Res.* 15, 178. <https://doi.org/10.1186/s12917-019-1925-6>.
- Lin, S.Y., Li, Y.T., Chen, Y.T., Chen, T.C., Hu, C.J., Chen, H.W., 2016. Identification of an infectious bronchitis coronavirus strain exhibiting a classical genotype but altered antigenicity, pathogenicity, and innate immunity profile. *Sci. Rep.* 6, 37725. <https://doi.org/10.1038/srep37725>.
- Lin, Y., Wu, F., Xie, Z., Song, X., Zhu, Q., Wei, J., Tan, S., Liang, L., Gong, B., 2020. [Clinical study of artesunate in the treatment of coronavirus disease 2019]. *Zhonghua Wei Zhong Bing Ji Jiu Yi Xue* 32, 417–420. <https://doi.org/10.3760/cma.j.cn121430-20200312-00412>.
- Liu, H., Wang, C., He, Y., Wei, X., Cheng, J., Yang, W., Shi, K., Si, H., 2024. Assessing a respiratory toxic infectious bronchitis virus (IBV) strain: isolation, identification, pathogenicity, and immunological failure insights. *Microbiol. Spectr.* 12, e0399023. <https://doi.org/10.1128/spectrum.0399023>.
- Liu, J., Li, D., Mei, J., Wu, L., Chen, F., Liu, Y., Lang, X., Yuan, G., Zhao, Y., 2022. [Analysis of prescription and medication rules of traditional Chinese medicine in the treatment of the coronavirus disease 2019 based on traditional Chinese medicine inheritance support platform]. *Zhonghua Wei Zhong Bing Ji Jiu Yi Xue* 34, 454–458. <https://doi.org/10.3760/cma.j.cn121430-20210907-01342>.
- Liu, S., Xiao, G., Wang, Q., Tian, J., Feng, X., Zhang, Q., Gong, L., 2023. Effects of dietary Astragalus membranaceus and Codonopsis pilosula extracts on growth performance, antioxidant capacity, immune status, and intestinal health in broilers. *Front. Vet. Sci.* 10, 1302801. <https://doi.org/10.3389/fvets.2023.1302801>.
- Luo, W., Brouwer, C., 2013. Pathview: an R/bioconductor package for pathway-based data integration and visualization. *Bioinformatics* 29, 1830–1831. <https://doi.org/10.1093/bioinformatics/btt285>.
- Lv, D., Dong, Z.H., Fan, W.S., Tang, N., Wang, L., Wei, L.P., Ji, Z.H., Tang, J.W., Lin, L.T., Wei, T.C., Huang, T., Wei, P., Mo, M.L., 2021. Identification of a novel avian coronavirus infectious bronchitis virus variant with three-nucleotide-deletion in



- nucleocapsid gene in China. *J. Vet. Med. Sci.* 83, 1608–1619. <https://doi.org/10.1292/jvms.21-0351>.
- Mahallawi, W.H., Khabour, O.F., Zhang, Q., Makhdom, H.M., Suliman, B.A., 2018. MERS-CoV infection in humans is associated with a pro-inflammatory Th1 and Th17 cytokine profile. *Cytokine* 104, 8–13. <https://doi.org/10.1016/j.cyto.2018.01.025>.
- Malumbres, M., Barbacid, M., 2009. Cell cycle, CDKs and cancer: a changing paradigm. *Nat. Rev. Cancer* 9, 153–166. <https://doi.org/10.1038/nrc2602>.
- Mei, Y., Li, L., Fan, L., Fan, W., Liu, L., Zhang, F., Hu, Z., Wang, K., Yang, L., Wang, Z., 2023. The history, stereochemistry, ethnopharmacology and quality assessment of borneol. *J. Ethnopharmacol.* 300, 115697. <https://doi.org/10.1016/j.jep.2022.115697>.
- Mork, A.K., Hesse, M., El Rahman, S.Abd, Rautenschlein, S., Herrler, G., Winter, C., 2014. Differences in the tissue tropism to chicken oviduct epithelial cells between avian coronavirus IBV strains QX and B1648 are not related to the sialic acid binding properties of their spike proteins. *Vet. Res.* 45, 67. <https://doi.org/10.1186/1297-9716-45-67>.
- Navarro-Reig, M., Jaumot, J., Garcia-Reiriz, A., Tauler, R., 2015. Evaluation of changes induced in rice metabolome by Cd and Cu exposure using LC-MS with XCMS and MCR-ALS data analysis strategies. *Anal. Bioanal. Chem.* 407, 8835–8847. <https://doi.org/10.1007/s00216-015-9042-2>.
- Niedernhofer, L.J., Daniels, J.S., Rouzer, C.A., Greene, R.E., Marnett, L.J., 2003. Malondialdehyde, a product of lipid peroxidation, is mutagenic in human cells. *J. Biol. Chem.* 278, 31426–31433. <https://doi.org/10.1074/jbc.M212549200>.
- Noor, F., Asif, M., Ashfaq, U.A., Qasim, M., Tahir Ul Qamar, M., 2023. Machine learning for synergistic network pharmacology: a comprehensive overview. *Brief Bioinform.* 24. <https://doi.org/10.1093/bib/bbad120>.
- Ogata, H., Goto, S., Sato, K., Fujibuchi, W., Bono, H., Kanehisa, M., 1999. KEGG: kyoto encyclopedia of genes and genomes. *Nucleic Acids Res.* 27, 29–34. <https://doi.org/10.1093/nar/27.1.29>.
- Pai, M., Er-Bu, A., Wu, Y., Ming, T.W., Gaun, T.K.W., Ye, B., 2023. Total alkaloids of bulbous of *Fritillaria cirrhosa* alleviate bleomycin-induced inflammation and pulmonary fibrosis in rats by inhibiting TGF-beta and NF-kappaB signaling pathway. *Food Nutr. Res.* 67. <https://doi.org/10.29219/fnr.v67.10292>.
- Pei, J., Sekellick, M.J., Marcus, P.I., Choi, I.S., Collisson, E.W., 2001. Chicken interferon type I inhibits infectious bronchitis virus replication and associated respiratory illness. *J. Interferon Cytokine Res.* 21, 1071–1077. <https://doi.org/10.1089/107999001317205204>.
- Peng, S., Fang, C., He, H., Song, X., Zhao, X., Zou, Y., Li, L., Jia, R., Yin, Z., 2022a. Myricetin exerts its antiviral activity against infectious bronchitis virus by inhibiting the deubiquitinating activity of papain-like protease. *Poult. Sci.* 101, 101626. <https://doi.org/10.1016/j.psj.2021.101626>.
- Peng, X., Wang, K., Wang, Y., Lu, Y., Lv, F., Cui, Y., Wang, Y., Si, H., 2022b. Exploration of the mechanism of the control of coccidiosis in chickens based on network pharmacology and molecular docking with the addition of modified Gegen Qinlian decoction. *Front. Vet. Sci.* 9, 849518. <https://doi.org/10.3389/fvets.2022.849518>.
- Pratiwi, R., Ramadhanti, S.P., Amatulloh, A., Megantara, S., Subra, L., 2023. Recent advances in the determination of veterinary drug residues in food. *Foods* 12. <https://doi.org/10.3390/foods12183422>.
- Qiu, J., Xiao, G., Yang, M., Huang, X., Cai, D., Xie, C., Chen, Z., Bi, X., Xu, A., 2023. Integrated network pharmacology and metabolomics reveal the mechanisms of jasmimum elongatum in anti-ulcerative colitis. *Sci. Rep.* 13, 22449. <https://doi.org/10.1038/s41598-023-49792-w>.
- Rasmussen, J.A., Villumsen, K.R., Ernst, M., Hansen, M., Forberg, T., Gopalakrishnan, S., Gilbert, M.T.P., Bojesen, A.M., Kristiansen, K., Limborg, M.T., 2022. A multi-omics approach unravels metagenomic and metabolic alterations of a probiotic and synbiotic additive in rainbow trout (*Oncorhynchus mykiss*). *Microbiome* 10, 21. <https://doi.org/10.1186/s40168-021-01221-8>.
- Ren, X., Guo, Y., Wang, H., Gao, X., Chen, W., Wang, T., 2023. The intelligent experience inheritance system for traditional Chinese medicine. *J. Evid. Based Med.* 16, 91–100. <https://doi.org/10.1111/jebm.12517>.
- Reynolds, D.L., Simpson, E.B., 2022. Evaluation of ivermectin antiviral activity against avian infectious bronchitis virus using a chicken embryo model. *Int. J. Vet. Sci. Med.* 10, 19–24. <https://doi.org/10.1080/23144599.2022.2050077>.
- Saxena, R., Chandra, V., Manohar, M., Hajela, K., Debnath, U., Prabhakar, Y.S., Saini, K. S., Konwar, R., Kumar, S., Megu, K., Roy, B.G., Dwivedi, A., 2013. Chemotherapeutic potential of 2-[Piperidinoethoxyphenyl]-3-phenyl-2H-benzo(b)pyran in estrogen receptor- negative breast cancer cells: action via prevention of EGFR activation and combined inhibition of PI-3-K/Akt/FOXO and MEK/Erk/AP-1 pathways. *PLoS One* 8, e66246. <https://doi.org/10.1371/journal.pone.0066246>.
- Schinkel, A.H., Jonker, J.W., 2003. Mammalian drug efflux transporters of the ATP binding cassette (ABC) family: an overview. *Adv. Drug Deliv. Rev.* 55, 3–29. [https://doi.org/10.1016/s0169-409x\(02\)00169-2](https://doi.org/10.1016/s0169-409x(02)00169-2).
- Su, Y., Chen, L., Yang, J., 2024. Hesperetin inhibits bladder cancer cell proliferation and promotes apoptosis and cycle arrest by PI3K/AKT/FoxO3a and ER stress-mitochondria pathways. *Curr. Med. Chem.* <https://doi.org/10.2174/010929867328388823121714702>.
- Sud, M., Fahy, E., Cotter, D., Brown, A., Dennis, E.A., Glass, C.K., Merrill Jr., A.H., Murphy, R.C., Raetz, C.R., Russell, D.W., Subramaniam, S., 2007. LMSD: LIPID MAPS structure database. *Nucleic Acids Res.* 35, D527–D532. <https://doi.org/10.1093/nar/gkl838>.
- Szakacs, G., Varadi, A., Ozvegy-Laczka, C., Sarkadi, B., 2008. The role of ABC transporters in drug absorption, distribution, metabolism, excretion and toxicity (ADME-Tox). *Drug Discov. Today* 13, 379–393. <https://doi.org/10.1016/j.drudis.2007.12.010>.
- Tang, S., Yang, H., 2024. Function and application of traditional Chinese medicine inheritance calculate system. *Sci. Tradit. Chin. Med.* 2, 66–69.
- Thevenot, E.A., Roux, A., Xu, Y., Ezan, E., Junot, C., 2015. Analysis of the human adult urinary metabolome variations with age, body mass index, and gender by implementing a comprehensive workflow for univariate and OPLS statistical analyses. *J. Proteome Res.* 14, 3322–3335. <https://doi.org/10.1021/acs.jproteome.5b00354>.
- Valastro, V., Holmes, E.C., Britton, P., Fusaro, A., Jackwood, M.W., Cattoli, G., Monne, I., 2016. S1 gene-based phylogeny of infectious bronchitis virus: an attempt to harmonize virus classification. *Infect. Genet. Evol.* 39, 349–364. <https://doi.org/10.1016/j.meegid.2016.02.015>.
- van Wietmarschen, H., van Steenberg, N., van der Werf, E., Baars, E., 2022. Effectiveness of herbal medicines to prevent and control symptoms of urinary tract infections and to reduce antibiotic use: a literature review. *Integr. Med. Res.* 11, 100892. <https://doi.org/10.1016/j.imr.2022.100892>.
- Vasilev, N., Boccard, J., Lang, G., Gromping, U., Fischer, R., Goepfert, S., Rudaz, S., Schillberg, S., 2016. Structured plant metabolomics for the simultaneous exploration of multiple factors. *Sci. Rep.* 6, 37390. <https://doi.org/10.1038/srep37390>.
- Wang, J., Zhang, Z., Li, R., Mao, F., Sun, W., Chen, J., Zhang, H., Bartsch, J.W., Shu, K., Lei, T., 2018. ADAM12 induces EMT and promotes cell migration, invasion and proliferation in pituitary adenomas via EGFR/ERK signaling pathway. *Biomed. Pharmacother.* 97, 1066–1077. <https://doi.org/10.1016/j.biopha.2017.11.034>.
- Wang, X., Liu, Z., 2014. Prevention and treatment of viral respiratory infections by traditional Chinese herbs. *Chin. Med. J.* 127, 1344–1350 (Engl).
- Wani, A.R., Yadav, K., Khursheed, A., Rather, M.A., 2021. An updated and comprehensive review of the antiviral potential of essential oils and their chemical constituents with special focus on their mechanism of action against various influenza and coronaviruses. *Microb. Pathog.* 152, 104620. <https://doi.org/10.1016/j.micpath.2020.104620>.
- Want, E.J., Masson, P., Michopoulos, F., Wilson, I.D., Theodoridis, G., Plumb, R.S., Shockcor, J., Loftus, N., Holmes, E., Nicholson, J.K., 2013. Global metabolic profiling of animal and human tissues via UPLC-MS. *Nat. Protoc.* 8, 17–32. <https://doi.org/10.1038/nprot.2012.135>.
- Wei, Y., Li, Y., Wang, S., Xiang, Z., Li, X., Wang, Q., Dong, W., Gao, P., Dai, L., 2023. Phytochemistry and pharmacology of armeniacae semen amarum: a review. *J. Ethnopharmacol.* 308, 116265. <https://doi.org/10.1016/j.jep.2023.116265>.
- Wiseman, N., 2002. Traditional Chinese medicine: a brief outline. *J. Chem. Inf. Comput. Sci.* 42, 445–455. <https://doi.org/10.1021/ci010107l>.
- Wishart, D.S., Tzur, D., Knox, C., Eisner, R., Guo, A.C., Young, N., Cheng, D., Jewell, K., Arndt, D., Sawhney, S., Fung, C., Nikolai, L., Lewis, M., Coutouly, M.A., Forsythe, I., Tang, P., Shrivastava, S., Jeronick, K., Stothard, P., Amegbey, G., Block, D., Hau, D. D., Wagner, J., Miniaci, J., Clements, M., Gebremedhin, M., Guo, N., Zhang, Y., Duggan, G.E., Macinnis, G.D., Weljie, A.M., Dowlatabadi, R., Bamforth, F., Clive, D., Greiner, R., Li, L., Marrie, T., Sykes, B.D., Vogel, H.J., Querengesser, L., 2007. HMDB: the human metabolome database. *Nucleic Acids Res.* 35, D521–D526. <https://doi.org/10.1093/nar/gkl923>.
- Xia, J., Wishart, D.S., 2011. Web-based inference of biological patterns, functions and pathways from metabolomic data using MetaboAnalyst. *Nat. Protoc.* 6, 743–760. <https://doi.org/10.1038/nprot.2011.319>.
- Xiang, X., Lv, J., Dong, M., Li, N., Li, Y., Wang, A., Shen, Y., Li, S., Xu, J., Cui, M., Han, X., Xia, J., Huang, Y., 2023. Radix Isatidis polysaccharide (RIP) resists the infection of QX-type infectious bronchitis virus via the MDA5/TLR3/IRF7 signaling pathway. *Poult. Sci.* 102, 102534. <https://doi.org/10.1016/j.psj.2023.102534>.
- Xu, J., Yin, P., Liu, X., Hou, X., 2023. Forsythoside A inhibits apoptosis and autophagy induced by infectious bronchitis virus through regulation of the PI3K/akt/NF-kappaB pathway. *Microbiol. Spectr.* 11, e0192123. <https://doi.org/10.1128/spectrum.01921-23>.
- Yamauchi-Takahara, K., Kishimoto, T., 2000. A novel role for STAT3 in cardiac remodeling. *Trends Cardiovasc. Med.* 10, 298–303. [https://doi.org/10.1016/s1050-1738\(01\)00066-4](https://doi.org/10.1016/s1050-1738(01)00066-4).
- Yang, R., Wang, L.Q., Yuan, B.C., Liu, Y., 2015. The pharmacological activities of licorice. *Planta Med.* 81, 1654–1669. <https://doi.org/10.1055/s-0035-1557893>.
- Yin, J., Li, G., Li, J., Yang, Q., Ren, X., 2011. *In vitro* and *in vivo* effects of Houttuynia cordata on infectious bronchitis virus. *Avian Pathol.* 40, 491–498. <https://doi.org/10.1080/03079457.2011.605107>.
- Yin, J., Ma, L., Wang, H., Yan, H., Hu, J., Jiang, W., Li, Y., 2017. Chinese herbal medicine compound Yi-Zhi-Hao pellet inhibits replication of influenza virus infection through activation of heme oxygenase-1. *Acta Pharm. Sin. B* 7, 630–637. <https://doi.org/10.1016/j.apsb.2017.05.006>.
- Yuan, S., Jiang, S.C., Zhang, Z.W., Fu, Y.F., Zhu, F., Li, Z.L., Hu, J., 2022. Abuse of amantadine in poultry may be associated with higher fatality rate of H5N1 infections in humans. *J. Med. Virol.* 94, 2588–2597. <https://doi.org/10.1002/jmv.27664>.
- Zelena, E., Dunn, W.B., Broadhurst, D., Francis-McIntyre, S., Carroll, K.M., Begley, P., O'Hagan, S., Knowles, J.D., Halsall, A., Consortium, H., Wilson, I.D., Kell, D.B., 2009. Development of a robust and repeatable UPLC-MS method for the long-term

- metabolomic study of human serum. *Anal. Chem.* 81, 1357–1364. <https://doi.org/10.1021/ac8019366>.
- Zhang, A.N., Li, N., Chen, Z.C., Guo, Y.L., Tian, C.J., Cheng, D.J., Tang, X.Y., Zhang, X.Y., 2023. Amygdalin alleviated TGF-beta-induced epithelial-mesenchymal transition in bronchial epithelial cells. *Chem. Biol. Interact.* 369, 110235. <https://doi.org/10.1016/j.cbi.2022.110235>.
- Zhang, X., Deng, T., Lu, J., Zhao, P., Chen, L., Qian, M., Guo, Y., Qiao, H., Xu, Y., Wang, Y., Li, X., Zhang, G., Wang, Z., Bian, C., 2020. Molecular characterization of variant infectious bronchitis virus in China, 2019: implications for control programmes. *Transbound. Emerg. Dis.* 67, 1349–1355. <https://doi.org/10.1111/tbed.13477>.
- Zhang, Y., Hou, J., Zeng, Z., 2022. Analysis of prescription medication rules of traditional Chinese medicine for diabetes treatment based on data mining. *J. Healthc. Eng.* 2022, 7653765. <https://doi.org/10.1155/2022/7653765>.